OPTICAL TRAPPING NANOMETRY OF HYPERMETHYLATED CPG-ISLAND DNA

Cs. I. Pongor, P. Bianco, Gy. Ferenczy, R. Kellermayer, M. Kellermayer

Key words: CpG island; optical tweezers; nanomechanics; overstretch transition; S-form DNA

Abstract

Cytosine methylation is a key mechanism of epigenetic regulation. CpG-dense loci, called CpG islands, play a particularly important role in modulating gene expression. Methylation has long been suspected to alter the physical properties of DNA, but the full spectrum of the evoked changes is unknown. Here we measured the methylation-induced nanomechanical changes in a DNA molecule with the sequence of a CpG island. For the molecule under tension, contour length, bending rigidity and intrinsic stiffness decreased in hypermethylated dsDNA, pointing at structural compaction which may facilitate DNA packaging *in vivo*. Intriguingly, increased forces were required to convert hypermethylated dsDNA into an extended S-form configuration. The reduction of force hysteresis during mechanical relaxation indicated that methylation generates a barrier against strand unpeeling and melting-bubble formation. The high structural stability is likely to have significant consequences on the recognition, replication, transcription and reparation of hypermethylated genetic regions.

Introduction

The chemical structure of DNA defines its nanomechanical properties, thereby strongly influencing the efficiency of DNA packaging and the activity of DNA-based mechanoenzymes. Methylation of cytosines in CpG dinucleotides of the genomic DNA is one of the most important epigenetic modifications in higher organisms (1-3). CpG-rich regions called CpG islands precede more than 70% of genes in human cells, which points at crucial, yet not fully understood regulatory functions (4). CpG islands in active promoter regions are mostly unmethylated, while in most of the loci with smaller CpG density these dinucleotides are methylated. Hypermethylation in gene promoter CpG islands is usually associated with suppressed expression of the associated gene (5). Recently it has been shown that in addition to CpG sites other, non-CpG cytosines may also be methylated and that they may also play a regulatory role in transcriptional silencing and differentiation of mammalian cells (6-10). Alterations in DNA methylation state by either hyper- (5, 11) or hypomethylation (12, 13) have been correlated with neoplastic transformation and aberrant embryonic development. Cytosine methylation has long been suspected to modulate DNA nanomechanical properties, thereby influencing the binding of associated proteins and nucleosomes (14-19). However, often contradictory findings were observed about the methylation-induced nanomechanical changes in DNA (18, 20-24). Initial cyclization kinetics experiments have not detected changes in the flexibility of exhaustively methylated DNA sequences (20). By contrast, a reduced local flexibility was measured in DNA oligonucleotides containing selectively methylated CpG sites (21). Different magnitudes of contour-length reduction and stiffening of methylated DNA were found by measuring the

equilibrium shape of surface-adsorbed molecules with atomic force microscopy (AFM) (22, 23, 25). By using molecular force assay and AFM-based pulling experiments, it has been shown that methylation significantly affects strand separation forces and thus DNA mechanical stability (24). Furthermore, DNA flexibility in chromatin may either increase or decrease depending on the nucleosomal positioning relative to the CpG dinucleotides (16, 26, 27). Altogether, prior findings indicate that methylation alters the mechanical properties of DNA. However, the overall spectrum of structural and dynamic alterations and the precise mechanisms of methylation-induced nanomechanical changes in DNA are still unclear.

Optical trapping nanometry (optical tweezers) is a sensitive method for characterizing the mechanical properties and force-driven transitions of individual DNA molecules (28-30). The ends of a DNA molecule can be captured with various available chemical techniques, and the molecule's structure is not constrained by interactions with surfaces. Upon stretching a double-stranded (ds) DNA molecule with optical tweezers, in the force range of 0-10 pN the molecule first extends at the expense of reducing its configurational entropy while the end-to-end distance asymptotically approaches the contour length. The measure of the molecule's bending rigidity is the persistence length, which may be obtained by fitting the experimental data with the wormlike chain (WLC) model of entropic elasticity (31). In the force range of 10-60 pN, in the so-called enthalpic regime, dsDNA extends due to the distortion of the bonds holding its structure together. The measure of axial elasticity in this regime is the stretch modulus (or intrinsic stiffness), which can be obtained by fitting the experimental data with a model of extensible wormlike chain (32, 33). At around 65 pN dsDNA cooperatively extends within a narrow force range to approximately 1.7 times its length (30). Three processes appear to proceed simultaneously within a torsionally unconstrained dsDNA molecule during this overstretch transition (34, 35): strand unpeeling, melting bubble formation, and transition into a so-called S-form configuration. Although the exact structure of S-form DNA is not known, it is hypothesized to be an unwound helix, much like a ladder, with base pairing intact. At forces above 65 pN the molecule displays the mechanical properties of either the S-form DNA, or, if strand separation has occurred, single-stranded (ss) DNA. Upon relaxing from the overstretched state, DNA recovers its structure very rapidly. Increasing levels of strand unpeeling and bubble formation, however, can impede the structural recovery, which is manifested in the appearance of force hysteresis (30, 34). By cyclically stretching and relaxing a dsDNA molecule with optical tweezers, the complex spectrum of its nanomechanical behavior may thus be characterized.

In the present work we explored the effect of methylation on the nanomechanical properties of a 3312-base-pair (bp)-long piece of DNA that met the criteria of a CpG island, by using optical trapping nanometry in the force range of 0-100 pN with high spatial (~1 nm) and force resolution (~0.2 pN). The use of both enzymatic and chemical methylation allowed us to assess the contribution of both CpG and the additional non-CpG cytosines to DNA nanomechanics. Hypermethylation led to the structural compaction, increased bending and axial compliance and the stabilization of the double-stranded DNA structure under tension. Furthermore, we find that in the overstretched state methylated DNA is longer than the non-methylated, suggesting that it attains a novel extended S-form. Hypermethylation-induced changes are thus likely to influence DNA packaging and the rates of DNA-based mechanoenzymatic processes.

Materials and methods

Sample preparation

A 3312-bp-long sequence was selected from λ-phage DNA by using a CpG island search algorithm (36, 37). Three different samples were prepared: a non-methylated sequence for use as control (DNA_{nm}), an enzymatically methylated sample (DNA_{em}) and a chemically methylated one (DNA_{cm}). DNA_{nm} was prepared with standard PCR employing DreamTaq polymerase (Fermentas, Vilnius, Lithuania). Primers (5'-biotin-CGTGCCGGTGTGCAG and 5'-NH_2-CACCGCTGGCGTTCA) were designed with the primer3 tool (38) using the entire λ-phage genome sequence available in the GeneBank (39) database (for further detail, see **Supporting information**). The resulting reaction mixtures were purified from agarose gel (1% agarose, Tris-acetate-EDTA buffer, 10 V/cm). The final product was isolated with a QIAprep Spin Miniprep kit and eluted with ultrapure water. DNA concentration was determined by measuring absorbance at 260 nm (Nanodrop 1000). Concentration was typically around 30 ng/µl. Purity, according to the 260/280 nm absorbance ratio, was approximately 1.8 in all cases. DNA_{em} was prepared by methylating DNA_{nm} with M.SssI CpG methyltransferase (Thermo Fisher Scientific Inc. Waltham, MA USA) by mixing 33 µl of 40 ng/µl DNA solution, 4 µl of 10x M.SssI Buffer, 2 µl of enzyme solution and 1 µl of 5mM S-adenosyl methionine (SAM). Reaction mixtures were incubated at 37 °C for 30 minutes, and the reaction was stopped by raising the temperature to 65 °C. DNA_{em} was purified and quantified similarly to DNA_{nm}. Methylation efficiency was assessed by digestion with the methylation-sensitive HpaII restriction enzyme (Fermentas,Vilnius, Lithuania) and by pyrosequencing. The tests indicated that nearly all (~90 %) cytosines in CpG sites became methylated, which corresponds to 15 % of all cysteines in the sequence (see **Supporting information**). In DNA_{cm} all cytosines were methylated (except for ten cytosines in the primers) regardless of whether C was in a CpG site or not. DNA_{cm} was prepared by adding m^5CTP, instead of CTP, to the standard PCR mixture. The reaction was optimized by adding 6-8 % DMSO to the reaction mixture (see **Supporting information**). Since the level of methylation (i.e., hypo- or hypermethylation) is expressed as a relative measure (i.e., in comparison to the usual methylation level of the given genetic region), because 90% of the CpG cytosines were methylated in DNA_{em} and all of the cytosines were methylated in DNA_{cm}, we consider both of them hypermethylated.

Optical trapping nanometry

Nanomechanical manipulation was carried out with a custom-built dual-beam counter-propagating optical tweezers apparatus (40-43) in constant velocity mode (in some experiments force was kept constant, see Supporting Information). The NH_2 end of the DNA molecule was covalently linked to a 2.5 µm carboxylated latex bead (Kisker Biotech GmbH, Steinfurt, Germany). The other end of the molecule was attached to a 3.0 µm carboxylated latex bead coated with streptavidin, which captured the biotinyl group. One of the beads was held in the optical trap while the other one with a micropipette embedded in a custom-built flow chamber mounted on a close-loop piezoelectric (PZT) stage (Nano-PDQ375, Mad City Labs, Madison, WI). DNA molecules were stretched by moving the micropipette away from the trap with a constant rate (typically 500 nm/s) with a step resolution of ~1 nm. Trap stiffness was ~0.2 pN/nm. Instrument control and data acquisition were managed by using custom-written LabView routines using (LabView v.7.1, National Instruments, Austin, TX). Force was measured by calculating the change in photonic momentum (44), with a resolution of ~0.2 pN and acquisition

rate of 1-5 kHz. Buffer condition was 50 mM Tris-HCl pH 8.0, 150 mM NaCl, 2 mM EDTA. In order to identify the zero-extension position in the displacement data, the micropipette-bead was pressed gently against the trapped bead either prior to or following the experiment. Molecular extension (z) was calculated by correcting displacement (s) according to force (F) and trap stiffness (κ) as

$$z = s - \frac{F}{\kappa}. \quad (1)$$

Data were processed with LabView and IgorPro (v.6.2.2.2, WaveMetrics, Lake Oswego, OR) and were smoothed to 100 Hz with a median filter.

Atomic Force Microscopy

The topographical structure of surface-adsorbed DNA molecules was assessed with non-contact-mode atomic force microscopy (Cypher, Asylum Research, Santa Barbara, CA) using silicon cantilevers (AC160TS, Olympus, Tokyo, Japan, nominal tip radius 7 nm, resonance frequency cca 300 kHz). Samples were deposited on freshly cleaved mica in a buffer containing 10 mM NaCl, 4 mM HEPES (pH 8) and 2 mM $MgCl_2$. After 10 minutes of incubation the mica surface was washed gently with a stream of ultrapure water and dried with a flow of high purity N_2. Data acquisition and analysis were carried out with the IgorPro 6 software suite (Wavemetrics, Lake Oswego, OR) and custom modules from Asylum Research (see also **Supporting information, Fig. S5**).

Force-field molecular dynamics simulation

The modeled DNA molecule was a 30-bp section taken from the experimentally studied sequence (see **Supporting information**) and contained a total 23 cytosines (8 in CpG and 15 non-CpG cytosines). In the hypermethylated model molecule ($mDNA_{cm}$) all of the cytosines were methylated on ^5C, whereas in the control ($mDNA_{nm}$) none of them. The structures were built with Maestro (45) in double-stranded B-DNA conformation. TIP3 water boxes with 65x65x220 Å size were added (46). Simulations were carried out with the CHARMM36 force field(47) using the NAMD 2.10 program (48). After equilibration, steered molecular dynamics simulations were performed with 150 pN constant force applied for 15 ns under NVT conditions. 10 sets of force-time data were averaged for both $mDNA_{nm}$ and $mDNA_{cm}$.

Data analysis

Each force (F) *versus* extension (x) curve obtained in the optical trapping nanometry experiments was fitted, by using the Marquardt-Levenberg non-linear least squares method, with the extensible wormlike-chain (eWLC) equation (32, 33)

$$x = L_0\left[1 - \frac{1}{2}\left(\frac{k_B T}{F L_p}\right)^{1/2} + \frac{F}{K}\right], \quad (2)$$

to obtain the contour length (L_0), persistence length (L_P) and intrinsic stiffness (stretch modulus, K) of the DNA molecules. In this equation k_B is Boltzmann's constant, and T is absolute temperature. The force *versus* extension curves for ssDNA and S-form DNA were simulated according to established procedures (35) adapted for the contour length of our constructs and for the ionic conditions or our experiments. The analysis of AFM data (for contour and persistence lengths) is detailed in the **Supporting Information**.

Results

Hypermethylated DNA constructs

The DNA sequence chosen for nanomechanical measurements was cloned from λ-phage DNA (**Fig. 1.a)**. Sequence selection was based on the criteria of the CpG island: GC content>50%, total length>200 bp, and observed-to-expected CpG dinucleotide ratio>0.6 (37). The chosen 3312-bp-long sequence contained CpG elements with an average frequency of 1/9 base pairs (49-51) (**Figs. 1.a, S1**). While the control, non-methylated sequence (DNA_{nm}) lacked methylated cytosines altogether, the enzymatically methylated sequence (DNA_{em}) contained 300 methylated CpG sites (~90 % of CpG cytosines, ~15 % of all cytosines, see **Supporting information**). All except ten (in the two primers) of the 1942 cytosines were methylated in the chemically methylated sequence (DNA_{cm}), prepared with PCR containing m^5C in the reaction mix (**Fig. S2**). The structural features of the different DNA constructs were analyzed by using atomic force microscopy (AFM) (**Figs. S5-7**). The contour length of the methylated forms was significantly smaller than that of the non-methylated (**Figs. S6.d-e**, **Table 1**). The persistence length of the methylated forms, measured with two different types of shape analysis (**Fig. S7**), was significantly greater than that of the non-methylated (**Table 1**).

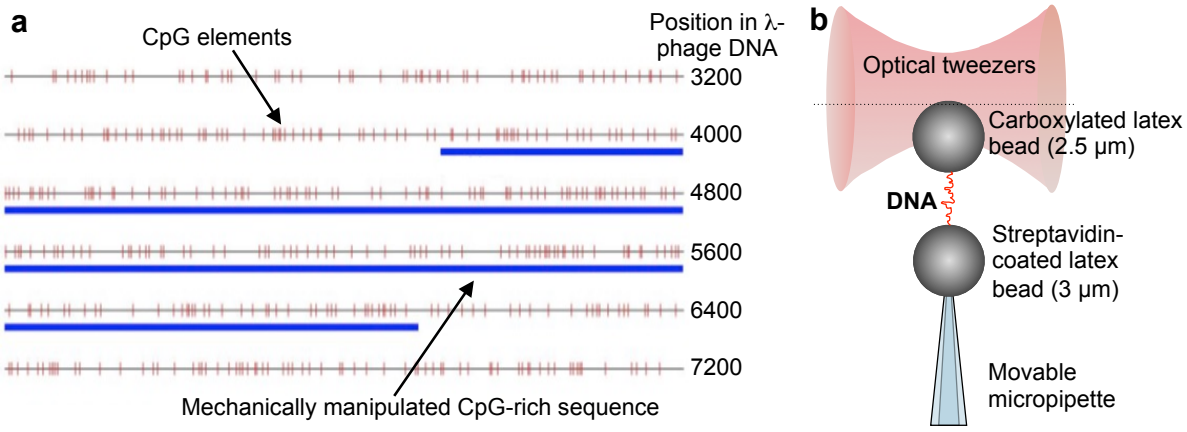

Figure 1. Nanomechanical manipulation of a CpG island. **a.** Layout of λ-phage DNA from position 2400 to 7200 illustrating the distribution of CpG elements (red bars). The CpG island chosen for our experiments is underlined in blue. **b.** Schematics of the optical trapping nanometry experiment.

Nanomechanics of differentially methylated dsDNA

We mechanically manipulated single molecules of dsDNA captured in a torsionally open geometry so as to maximize the conformational degrees of freedom. One of the 5' ends contained an NH_2 group, by which DNA was covalently attached to a carboxylated latex bead. The opposite 5' end contained biotin, by which this end was attached to a streptavidin-coated latex bead. Individual DNA molecules were manipulated with force-measuring optical tweezers (40-

43) by stretching and relaxing them with a constant velocity of 500 nm/s (**Fig. 1.b**). Nanomechanical data were collected in the force range of 0-100 pN. **Fig. 2** shows raw and superimposed smoothed stretch force *versus* extension data for DNA_{nm} (**Fig. 2.a**), DNA_{em} (**Fig. 2.b**) and DNA_{cm} (**Fig. 2.c**).

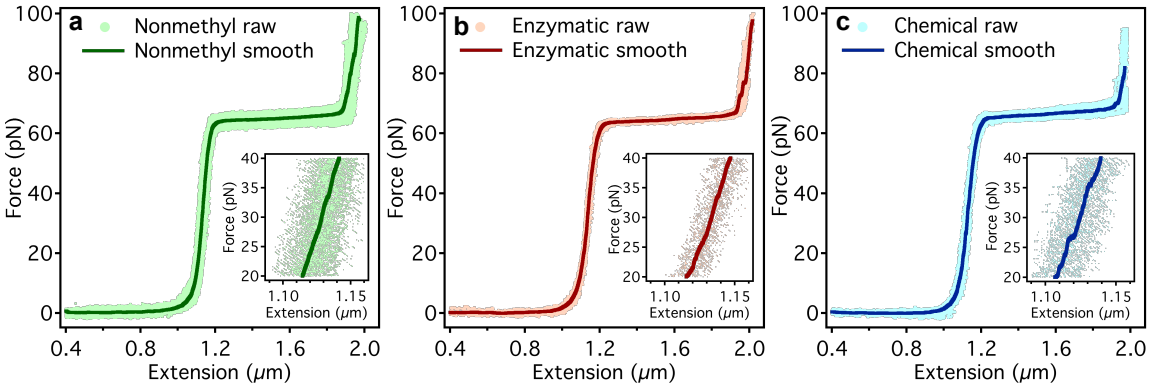

Figure 2. Force *versus* extension curves for the three different DNA forms. Raw data with superimposed smoothed data are shown. Smoothing was carried out by local averaging within a window the size of which was approximately 1% of the total dataset. **a.** Non-methylated DNA (DNA_{nm}). Raw data for 30 force *versus* extension curves containing a total number of 247 thousand datapoints are shown (light green points). Smoothing window was 2000 points wide. **b.** Enzymatically methylated DNA (DNA_{em}). Raw data for 17 force *versus* extension curves containing a total number of 65 thousand datapoints are shown (light red points). Smoothing window was 500 points wide. **c**. Chemically hypermethylated DNA (DNA_{cm}). Raw data for 15 force *versus* extension curves containing a total number of 101 thousand datapoints are shown (light blue points). Smoothing window was 1000 points wide. **Insets** show enlarged regions of the plots merely to indicate the dispersion of the data. In generating the above plots only stretch data were used.

The global appearance of the force-curves was similar for each DNA form. At low forces, a non-linear force response was observed, and at 65 pN a force plateau appeared that corresponds to the co-operative transition, which converts dsDNA into an overstretched state (30). Further stretch resulted in a sharp increase of force. To reveal the fine detail of differences in the nanomechanical behavior of the different DNA forms, we overlaid their consensus force *versus* extension curves (**Fig. 3**) and calculated the relevant polymer-chain parameters by fitting raw data with the extensible wormlike-chain (eWLC) model (equation 2) (**Table 1**). In the entropic regime (0-10 pN), subtle differences were observed between the non-methylated and methylated forms of dsDNA (**Fig. 3.b**). The contour and persistence lengths of $dsDNA_{em}$ were not significantly different from those of $dsDNA_{nm}$. In contrast, both the contour length and the persistence length were significantly reduced in $dsDNA_{cm}$ (**Table 1**). Significant changes were detected in the enthalpic regime of elasticity (10-60 pN), which describes extensibility beyond the contour length of the random, entropic polymer coil (**Fig. 3.c**). The stretch modulus of both $dsDNA_{em}$ and $dsDNA_{cm}$ was significantly smaller than that of $dsDNA_{nm}$ (**Table 1**).

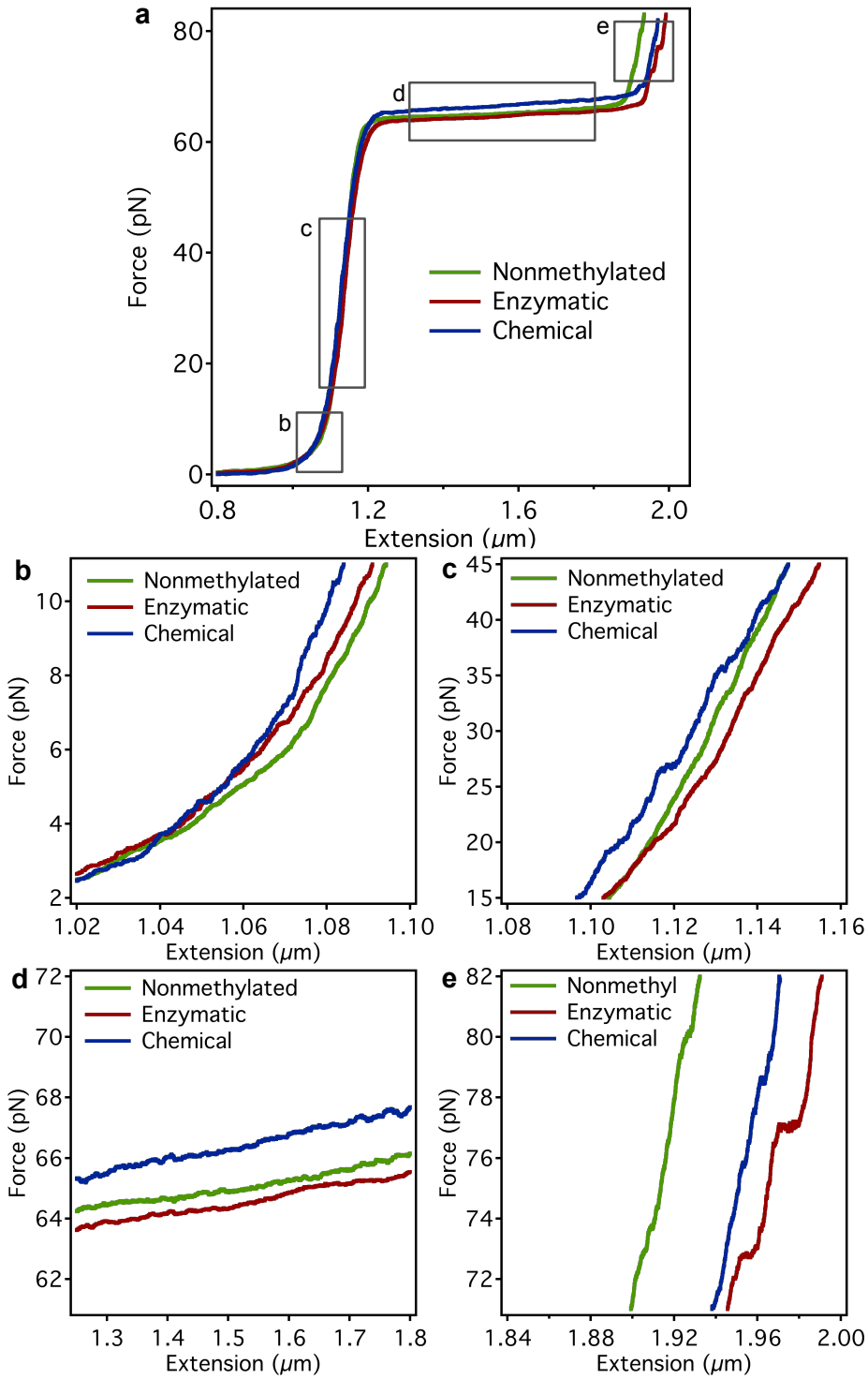

Figure 3. Comparison of nanomechanical data in different force regimes. **a.** Overview of the consensus force *versus* extension curves of the different DNA constructs. Boxes indicate the regions magnified in **b-e**. **b.** Region of dsDNA entropic elasticity. **c.** Region of dsDNA enthalpic elasticity. **d.** Overstretch transition. **e.** Region of the elastic behavior of overstretched DNA.

	Non-methylated DNA	Enzymatically methylated DNA	Chemically hypermethylated DNA
dsDNA Contour length (theoretical, 3.4 Å/bp)	1126.1	-	-
dsDNA Contour length, nm (AFM)	1089.4 ± 2.8 n=32	1056.8 ± 2.9 n=38	1059.3 ± 2.0 n=45
dsDNA persistence length, nm (AFM, mean-square-separation)	66.9 ± 0.3 n=32	78.8 ± 0.7 n=46	79.4 ± 0.4 n=58
dsDNA persistence length, nm (AFM, orientation correlation)	60.7± 0.2 n=34	71.2 ± 0.3 n=46	71.8 ± 0.3 n=58
dsDNA contour length, nm (optical tweezers, eWLC fit)	1142.5 ± 1.6 n=34	1143.3 ± 1.6 n=36	1132.2 ± 2.7 n=23
dsDNA persistence length, nm (optical tweezers, eWLC fit)	44.6 ± 1.5 n=34	41.2 ± 1.5 n=35	39.1 ± 1.8 n=23
dsDNA stretch modulus, pN (optical tweezers, eWLC fit)	1828.5 ± 52.5 n=34	1602.9 ± 53.2 n=36	1514.5 ± 66.3 n=23
Overstretch force, pN (at 1.5 µm extension)	64.1 ± 0.2 n=33	63.9 ± 0.2 n=17	66.2 ± 0.3 n=22
Overstretch transition slope, pN/µm (linear fit)	3.2 ± 0.1 n=30	3.6 ± 0.2 n=14	5.0 ± 0.5 n=15
S-DNA contour length, nm (eWLC fit)	1978.7 ± 8.7 n=33	2010.3 ± 5.4 n=35	2024.8 ± 8.9 n=16
Hysteresis length, nm (along overstretch transition)	160.4 ± 11.3 n=60	96.1 ± 8.7 n=105	11.4 ± 2.3 n=138
Hysteresis area, pNnm	1898.3 ± 448.28 n=17	688.57 ± 259.93 n=18	320.76 ± 30.824 n=14

Table 1. Structural and mechanical parameters of non-methylated, enzymatically and chemically hypermethylated DNA obtained in AFM and optical tweezers measurements. Errors refer to standard error of the mean except for the AFM-based persistence length data (standard deviation of the fit, see **Supporting Information**). n refers to the number of DNA molecules.

Force-induced overstretch transition

In the overstretch region (**Fig. 3.d**) of the force *versus* extension curves intriguing differences were observed between the non-methylated and methylated DNA forms. Differences were observed in three parameters: overstretch force, co-operativity and the length of the overstretch transition. While the overstretch force (measured at 1.5 µm extension that corresponds approximately to the midpoint of the transition) was not significantly different between DNA_{nm} and DNA_{em}, significantly greater forces were required to progress through this transition in the case of DNA_{cm} (**Fig. 3.d**, **Fig. 4.a**, **Table 1**). To estimate the co-operativity of the process, we measured the slope of the line fitted to the overstretch transition. The slope was significantly greater in both DNA_{em} and DNA_{cm} than in DNA_{nm} (**Fig. 4.b**, **Table 1**).

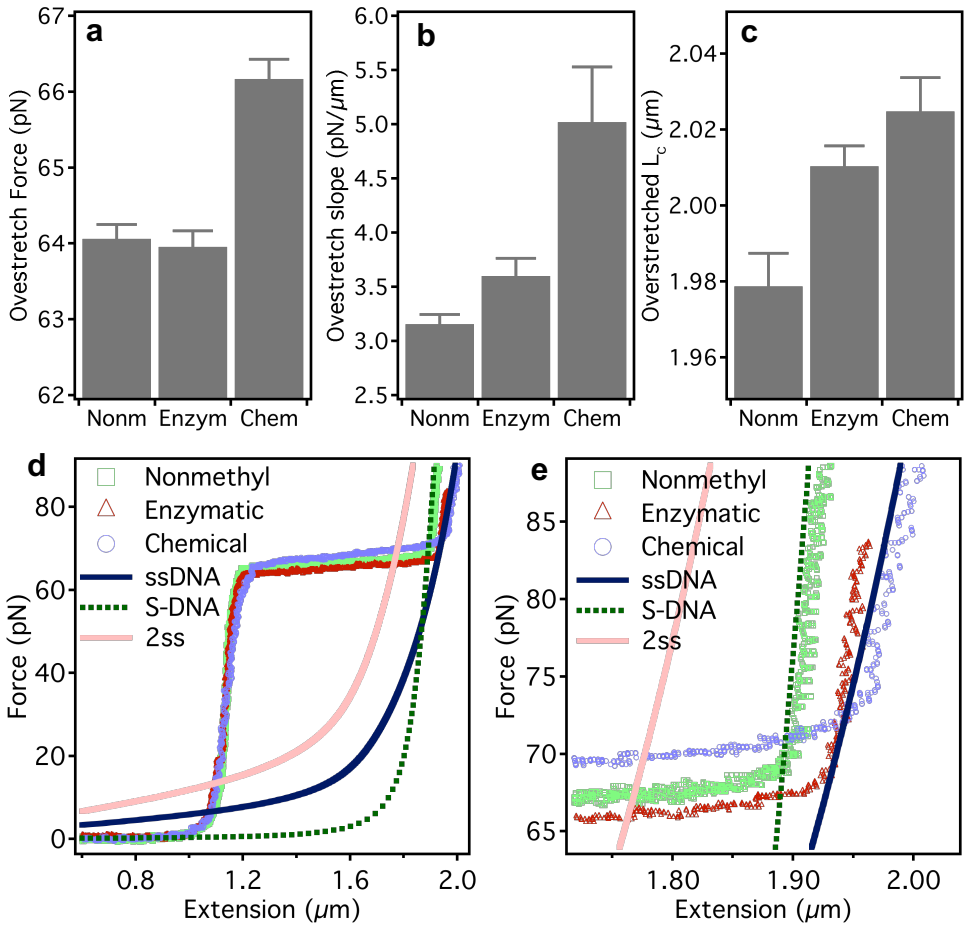

Figure 4. Overstretch behavior of dsDNA. **a.** Overstretch force, measured at 1.5 μm extension. **b.** Overstretch slope measured by fitting a line on the entire overstretch transition. **c.** Contour length of the overstretched DNA measured by fitting the eWLC equation on the force data. Stretch modulus of 2700 pN was systematically used in these fits. Detailed statistics are listed in **Table 1**. **d.** Comparison of experimental data with theoretical models of ssDNA, 2ssDNA and S-DNA. **e.** Enlarged view of **d** to highlight differences.

Finally, and most strikingly, the length of the transition was greater than that of DNA_{nm} in both methylated DNA forms, which resulted in an overstretched form of DNA with an extended contour length (**Fig. 3.e, Fig. 4.c, Table 1**). To explore the nature of the overstretched state, we compared representative force *versus* extension curves with theoretical data for S-form DNA, ssDNA and 2ssDNA (two ssDNA molecules held in parallel) (**Fig. 5.d-e**). According to the fit, overstretched DNA_{nm} resembled S-DNA, whereas overstretched methylated DNA forms were similar, apparently, to a ssDNA (**Fig. 5.d-e**). The 2ssDNA model showed a behavior entirely different from each of the different DNA constructs. Importantly, a truly single-stranded state is not possible under our experimental conditions, because DNA was captured at its opposite 5' ends in a torsionally open geometry. To investigate whether the overstretched state of methylated DNA corresponds to an alternative structure, we carried out repetitive stretch-relaxation cycles interrupted with pauses at high, clamped forces (**Figs 5, S8-11**). During stretch, only the co-operative overstretch transition was observed, and additional distinct transitions were never

detected. During relaxation, different mechanical behavior was observed depending on the methylation state. Whereas in DNA_{nm} a large hysteresis was typically observed (**Fig. 5.a**), force hysteresis was reduced in DNA_{em} (**Fig. 5.b**) and it was essentially absent in DNA_{cm} (**Fig. 5.c**). When held at a high constant force (>70 pN, 5 s), the extension of the DNA_{nm} and DNA_{em} slowly increased as a function of time, whereas that of the chemically hypermethylated form (DNA_{cm}) remained essentially constant (**Fig. S11**).

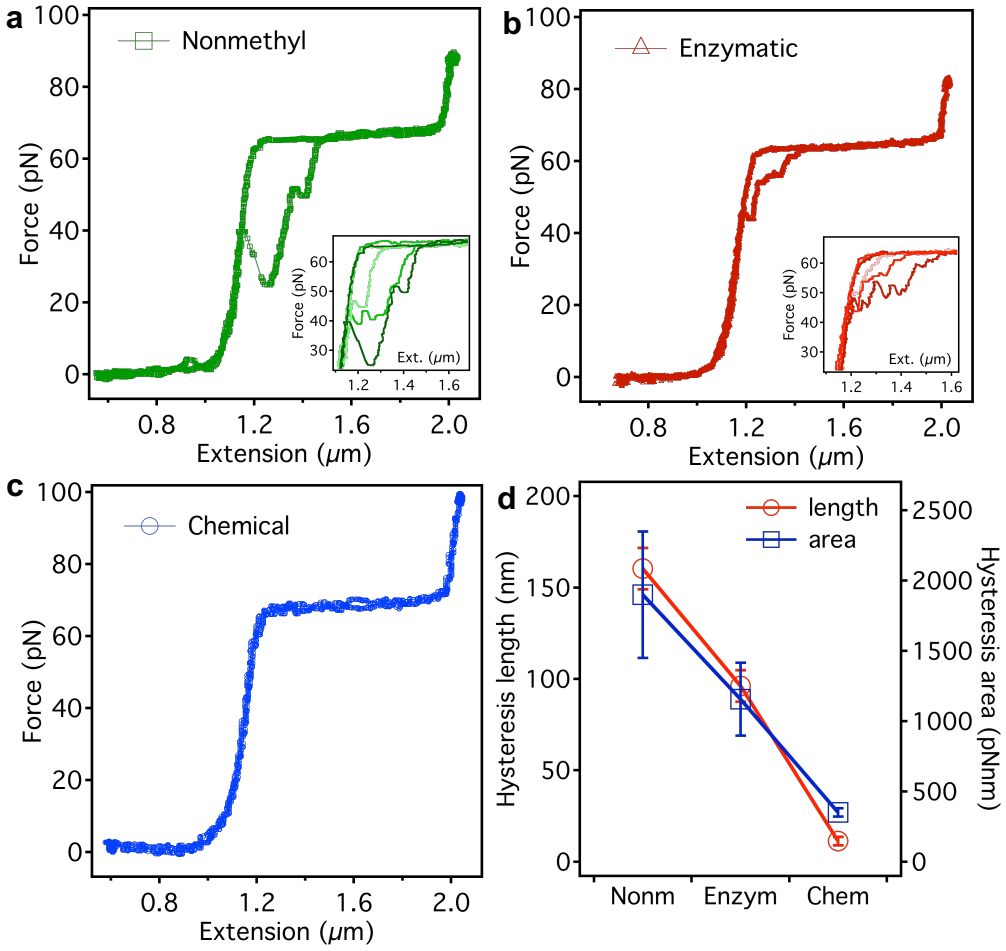

Figure 5. Analysis of force hysteresis. **a-c.** Force *versus* extension curves obtained in stretch and relaxation cycles for a DNA_{nm}, DNA_{em} and DNA_{cm} molecule. Single nanomechanical cycles are shown for each construct. Insets in a-b show magnified views of several force-extension cycles to indicate the hysteresis shape. **d.** Magnitude of hysteresis, measured as the length of the hysteretic region along the extension axis and as hysteresis area, as a function of methylation status. Detailed statistics are listed in **Table 1**.

Molecular dynamics simulation

To assess the structural basis of the nanomechanical differences between non-methylated and hypermethylated dsDNA, steered molecular dynamics simulations were carried out (**Fig. 6**, **Supplementary video**). Constant-force (extension *versus* time) rather than constant-velocity (force *versus* extension) simulations were performed for three reasons. First, because of its smaller computational demand, statistically meaningful number of simulation runs could be obtained that allowed averaging the data that contained large fluctuations. Second, the problems associated with the vast differences between loading rates in simulated *versus* experimental loading rates in constant-velocity manipulations could be minimized. Third, because of the small size (30 bp) of the model DNA molecules (mDNA), detectable length differences were anticipated only between the overstretch transitions of the non-methylated ($mDNA_{nm}$) and chemically hypermethylated ($mDNA_{cm}$) forms, where a large length change occurs across a narrow force range (see **Fig. 3.d**). Molecular structure snapshots of the simulation (**Fig. 6.a**) indicate that $mDNA_{cm}$ retains a greater helicity than $mDNA_{nm}$.

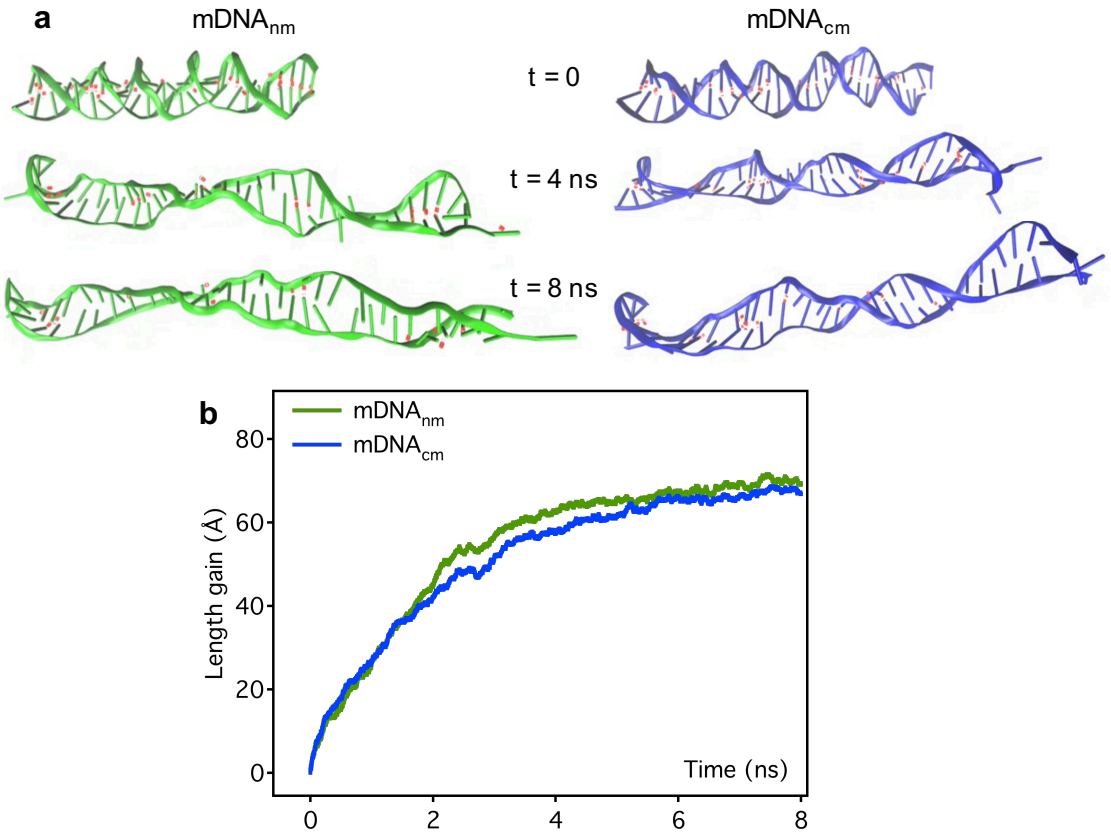

Figure 6. Force-field molecular dynamics simulation of non-methylated and hypermethylated model DNA (mDNA) constructs. **a.** Structures of the non-methylated ($mDNA_{nm}$) and hypermethylated ($mDNA_{cm}$) model DNA molecules at the highlighted time points during constant-force (150 pN) simulation. **b.** Length *versus* time functions for $mDNA_{nm}$ and $mDNA_{cm}$. The curves were obtained by averaging ten independent simulation runs. For further statistics, see **Supporting information**.

The averaged extension *versus* time curves (**Figs 6.b, S9**) indicate that the largest difference between the simulated nanomechanical behavior of $mDNA_{nm}$ and $mDNA_{cm}$ occurs in the 2-4 ns interval, which corresponds to 50-60% molecular extension. In this regime the extension of $mDNA_{cm}$ under the same force is smaller than that of $mDNA_{nm}$, indicating that greater force is required to stretch hypermethylated DNA than the non-methylated form. Considering that the 2-4 ns region corresponds to the overstretch transition (*c.f.* **Figs 3.a** and **d**), the simulation supports the experimental observations and provides a glimpse at the differences between the structures of the DNA forms.

Discussion

We have investigated the effect of methylation on DNA nanomechanics by using a 3312-bp model dsDNA that fulfilled the criteria of a CpG island, as opposed to the short arbitrary sequences in prior studies (18, 21, 24, 52). To maximize the effect of methylation, a PCR-based chemical protocol was used in addition to enzymatic treatment. The degree of cytosine modification reached hypermethylation levels in both DNA_{em} and DNA_{cm}. A further advantage of DNA_{cm} lies in the fact that it enables the assessment of non-CpG cytosine methylation as well. The structural features of the DNA constructs were characterized with AFM. The contour length of all three constructs was shorter than theoretically predicted (assuming 3.4Å/bp for B-DNA) in accordance with previous findings (53). In addition, according to our analysis, the contour length of the methylated DNA constructs was 3% shorter than that of the non-methylated form (**Fig. S6, Table 1**). Contour-length reduction in surface-adsorbed molecules of methylated DNA has been observed before (22). The persistence length of the surface-adsorbed methylated forms increased significantly (**Fig. S7, Table 1**) as reported before (22, 25). The observed stiffening is thought to be due to the dehydration of the hydrophobic hypermethylated DNA on the substrate interface (22). Under tension, however, the DNA molecule may display nanomechanical parameters different from those extracted by using shape analysis (54). Therefore, we exposed the DNA constructs to a wide range of forces that covered both the entropic and enthalpic elasticity regimes and the overstretch transition. Previous studies reported on the effect of methylation either only on its entropic elasticity or strand separation forces (22-24). Here, we were able to sensitively investigate the full spectrum of differences between the nanomechanics of non-methylated and methylated DNA.

In the force regime of entropic elasticity (0-10 pN), hypermethylation-evoked nanomechanical changes were subtle, but significant. The contour length of $dsDNA_{cm}$, as obtained from the optical tweezers data, was reduced by 1% (**Table 1**), indicating that hypermethylation indeed leads to an axial compaction of the DNA structure. In contrast to the AFM data, however, the persistence length of $dsDNA_{cm}$ became reduced, indicating that, apparently, methylation leads to an increase in the flexibility of the DNA chain under tension. Thus, smaller energy is required to bend dsDNA, which is likely to influence chain packaging by nucleosomes. We note that the persistence length of the non-methylated DNA construct was much smaller when measured with optical tweezers than with AFM. Such a difference has been noted before and has been attributed to a high (>50 %) GC content (54). The 59 % GC content of the DNA construct used in our experiments thus explains the persistence-length differences in DNA_{nm} observed with the different methods. The increased flexibility of methylated DNA under tension is in contrast with

some cyclization kinetics (18, 21) and AFM (22, 25) experiments which reported the stiffening of methylated DNA. We speculate that in cyclization kinetics a strong sequence dependence relative to the small size of the molecules (55), and in AFM experiments surface constraints and electrostatic effects (56) contribute to the observed differences. Furthermore, the differences may be reconciled by the increased enthalpic compliance observed here for the methylated DNA constructs (see **Fig. 3.c** and text below), which results in enhanced extensibility in the enthalpic regime of forces.

In the enthalpic regime of elasticity (10-60 pN) significantly smaller stretch moduli were determined for the methylated forms of DNA than for $dsDNA_{nm}$. Enthalpic or intrinsic elasticity is commonly attributed to the elastic distortion of bonds along DNA (28). It has been suggested that methylation generates angular distortions in the DNA backbone (20), which are then straightened during stretch. The smaller stretch moduli observed for the methylated DNA forms indicate that smaller forces are required for extending DNA in the 10-60 pN regime. Presumably, the greater axial compliance of methylated DNA further aids its packaging by nucleosomes.

The largest effect of hypermethylation was observed in the overstretch transition of the CpG island. Recently it has been shown that three processes may simultaneously occur during this process: strand unpeeling (denaturation) resulting in an apparent ssDNA behavior, melting-bubble formation that corresponds to local regions of partial inside-strand separation, and transition from the B-form into an S-form DNA (34, 35, 57). While the exact structure of S-DNA is still unknown, it is most commonly thought to resemble an unwound helix with a straightened configuration in which the coupling between the complementary strands is maintained (35). Because of the torsionally open geometry of our single-molecule manipulation experiment, all of the transitions were allowed to take place during stretch. However, we have not observed the distinct, stepwise, sawtooth-like transitions characteristic of strand unpeeling in any of the DNA constructs (34, 58). The absence of strand unpeeling is most likely caused by the overwhelming GC content of the constructs (59 %), which tends to stabilize the double-stranded configuration (58, 59). Comparison of the experimental data with theoretical models (**Fig. 4.d-e**) suggested that the overstretched state of DNA_{nm} is S-form DNA. The systematic presence of force hysteresis in DNA_{nm} indicates, furthermore, that melting-bubble formation was also present. Thus, the configuration of overstretched DNA_{nm} is a combination of S-DNA and melting bubbles. The gradual disappearance of force hysteresis caused by methylation (**Fig. 5**) suggests that the number of melting bubbles became progressively reduced, and the overstretched state of DNA_{em} and DNA_{cm} is dominated by S-form DNA. The lack of progressive extension of DNA_{cm} in high-force-clamp (>70 pN) experiments (**Fig. S11**) indicates that melting-bubble formation is strongly inhibited by methylation. In hypermethylated DNA, two significant differences were systematically observed in comparison with DNA_{nm}: the slope of the transition was increased, and the overstretched state was longer. Furthermore, in DNA_{cm}, hence due to non-CpG cytosine methylation, greater forces were required to evoke the overstretch transition. The elevated transition force indicates that a larger overall energy barrier needs to be surpassed during overstretch. Force-field molecular dynamics simulations on a short segment of the experimentally manipulated DNA (**Fig. 6**) supported the findings. Because the model DNA is ~1000-fold shorter than the one experimentally manipulated, the ~5 Å greater extension of $mDNA_{cm}$ than that of $mDNA_{nm}$ during the overstretch transition (**Fig. 6.b**, in the 2-4 ns time interval) corresponds remarkably well to the ~0.5 μm greater extension of DNA_{nm} than that of

DNA_{cm} in the optical tweezers experiment (**Fig. 3.d**, at ~65 pN). The increased overall energy barrier is likely due to stronger intrachain interactions caused by the increased hydrophobicity of the methylcytosines. The increased strand separation forces measured, by using molecular force assay, for more extensively methylated dsDNA (24) and the increased thermal stability of non-CpG-methylated dsDNA support this idea (60). The increase in the slope of the overstretch transition indicates that co-operativity became reduced. Thus, the number of sites along the DNA strand at which B-S transition coincidentally occurs becomes reduced upon methylation. Comparison of the experimental data with theoretical models (**Fig. 4.d-e**) suggested that the overstretched state of both DNA_{em} and DNA_{cm} resembles ssDNA. However, because of the lack of unpeeling transitions, the minimal or totally absent force hysteresis and the torsionally open geometry of the manipulated DNA, we exclude the possibility that the overstretched state of methylated DNA is true ssDNA. Rather, an extended S-form DNA is present. Assuming that the transition is homogenous along the DNA molecule, the extension involves a 0.14 Å/bp lengthening relative to S-form DNA. The structure of this extended S-DNA is not known. We speculate that a higher hydrogen bond distortion and a decreased helicity of the S-DNA form may underlie the extension transition. The significant reduction of hysteresis (**Fig. 5**) indicates that interstrand bonds are strengthened significantly. Possibly, the electron-donor properties of the methyl group enhance base stacking interactions that stabilize strand pairing in the stretched state. The longer-lived base pairing in the simulated $mDNA_{cm}$ molecule (**Fig. 6**, **Supplementary video**) supports this possibility. Furthermore, a base-paired but overstretched DNA conformation has recently been demonstrated in a GC-rich construct (61).

In conclusion, a putative novel form of extended S-DNA has been detected in the hypermethylated CpG island studied here. While the hypermethylated double-stranded CpG island may be packaged into a more compact configuration, it appears to be more difficult to separate its strands. Methylation of non-CpG cytosines apparently provide an additional stabilizing mechanism. Because strand separation is important in DNA replication, transcription and repair, hypermethylated CpG islands may present a thermodynamic and kinetic barrier for mechanoenzyme action. Slowing or halting mechanoenzymatic processes at hypermethylated CpG islands may thus contribute to a finely tuned spatial pattern of gene expression.

Author contributions

C.I.P. performed research, analyzed data, wrote paper; P.B. performed research; G.F. performed research; R.K. designed research, wrote paper; M.K. designed research, analyzed data, wrote paper.

Acknowledgements

This work was supported by grants from the Hungarian Science Foundation (OTKA **K109480**) and the National Research, Development and Innovation Office (**VKSZ_14-1-2015-0052**). The research leading to these results has received funding from the European Union's Seventh Framework Program (FP7/2007-2013) under grant agreement n° **HEALTH-F2-2011-278850 (INMiND)**. We gratefully acknowledge the assistance of Péter Hollósi of the 1st Department of

Pathology and Experimental Cancer Research, Semmelweis University, in the pyrosequencing measurements. We thank Hedvig Tordai and Carlos Bustamante for providing insightful suggestions during various stages of manuscript preparation.

References

1. Bird, A. 2002. DNA methylation patterns and epigenetic memory. Genes & development 16:6-21.
2. Jones, P. A., and D. Takai. 2001. The role of DNA methylation in mammalian epigenetics. Science 293:1068-1070.
3. Ehrlich, M., M. A. Gama-Sosa, L. H. Huang, R. M. Midgett, K. C. Kuo, R. A. McCune, and C. Gehrke. 1982. Amount and distribution of 5-methylcytosine in human DNA from different types of tissues of cells. Nucleic acids research 10:2709-2721.
4. Saxonov, S., P. Berg, and D. L. Brutlag. 2006. A genome-wide analysis of CpG dinucleotides in the human genome distinguishes two distinct classes of promoters. Proceedings of the National Academy of Sciences of the United States of America 103:1412-1417.
5. Jones, P. A., and S. B. Baylin. 2002. The fundamental role of epigenetic events in cancer. Nature reviews. Genetics 3:415-428.
6. Chen, L., K. Chen, L. A. Lavery, S. A. Baker, C. A. Shaw, W. Li, and H. Y. Zoghbi. 2015. MeCP2 binds to non-CG methylated DNA as neurons mature, influencing transcription and the timing of onset for Rett syndrome. Proceedings of the National Academy of Sciences of the United States of America 112:5509-5514.
7. Guo, J. U., Y. Su, J. H. Shin, J. Shin, H. Li, B. Xie, C. Zhong, S. Hu, T. Le, G. Fan, H. Zhu, Q. Chang, Y. Gao, G. L. Ming, and H. Song. 2014. Distribution, recognition and regulation of non-CpG methylation in the adult mammalian brain. Nat Neurosci 17:215-222.
8. Kinde, B., H. W. Gabel, C. S. Gilbert, E. C. Griffith, and M. E. Greenberg. 2015. Reading the unique DNA methylation landscape of the brain: Non-CpG methylation, hydroxymethylation, and MeCP2. Proceedings of the National Academy of Sciences of the United States of America 112:6800-6806.
9. Lister, R., M. Pelizzola, Y. S. Kida, R. D. Hawkins, J. R. Nery, G. Hon, J. Antosiewicz-Bourget, R. O'Malley, R. Castanon, S. Klugman, M. Downes, R. Yu, R. Stewart, B. Ren, J. A. Thomson, R. M. Evans, and J. R. Ecker. 2011. Hotspots of aberrant epigenomic reprogramming in human induced pluripotent stem cells. Nature 471:68-73.
10. Ramsahoye, B. H., D. Biniszkiewicz, F. Lyko, V. Clark, A. P. Bird, and R. Jaenisch. 2000. Non-CpG methylation is prevalent in embryonic stem cells and may be mediated by DNA methyltransferase 3a. Proceedings of the National Academy of Sciences of the United States of America 97:5237-5242.
11. Herman, J. G., and S. B. Baylin. 2003. Gene silencing in cancer in association with promoter hypermethylation. The New England journal of medicine 349:2042-2054.
12. Hanada, M., D. Delia, A. Aiello, E. Stadtmauer, and J. C. Reed. 1993. bcl-2 gene hypomethylation and high-level expression in B-cell chronic lymphocytic leukemia. Blood 82:1820-1828.
13. Daura-Oller, E., M. Cabre, M. A. Montero, J. L. Paternain, and A. Romeu. 2009. Specific gene hypomethylation and cancer: new insights into coding region feature trends. Bioinformation 3:340-343.
14. Gromiha, M. M. 2005. Influence of DNA stiffness in protein-DNA recognition. Journal of biotechnology 117:137-145.

15. Hogan, M. E., and R. H. Austin. 1987. Importance of DNA Stiffness in Protein DNA-Binding Specificity. Nature 329:263-266.
16. Osakabe, A., F. Adachi, Y. Arimura, K. Maehara, Y. Ohkawa, and H. Kurumizaka. 2015. Influence of DNA methylation on positioning and DNA flexibility of nucleosomes with pericentric satellite DNA. Open Biol 5.
17. Pennings, S., J. Allan, and C. S. Davey. 2005. DNA methylation, nucleosome formation and positioning. Briefings in functional genomics & proteomics 3:351-361.
18. Perez, A., C. L. Castellazzi, F. Battistini, K. Collinet, O. Flores, O. Deniz, M. L. Ruiz, D. Torrents, R. Eritja, M. Soler-Lopez, and M. Orozco. 2012. Impact of methylation on the physical properties of DNA. Biophysical journal 102:2140-2148.
19. Virstedt, J., T. Berge, R. M. Henderson, M. J. Waring, and A. A. Travers. 2004. The influence of DNA stiffness upon nucleosome formation. Journal of structural biology 148:66-85.
20. Hodges-Garcia, Y., and P. J. Hagerman. 1995. Investigation of the influence of cytosine methylation on DNA flexibility. The Journal of biological chemistry 270:197-201.
21. Nathan, D., and D. M. Crothers. 2002. Bending and flexibility of methylated and unmethylated EcoRI DNA. Journal of molecular biology 316:7-17.
22. Kaur, P., B. Plochberger, P. Costa, S. M. Cope, S. M. Vaiana, and S. Lindsay. 2012. Hydrophobicity of methylated DNA as a possible mechanism for gene silencing. Phys Biol 9.
23. Wanunu, M., D. Cohen-Karni, R. R. Johnson, L. Fields, J. Benner, N. Peterman, Y. Zheng, M. L. Klein, and M. Drndic. 2011. Discrimination of methylcytosine from hydroxymethylcytosine in DNA molecules. Journal of the American Chemical Society 133:486-492.
24. Severin, P. M., X. Zou, H. E. Gaub, and K. Schulten. 2011. Cytosine methylation alters DNA mechanical properties. Nucleic acids research 39:8740-8751.
25. Cassina, V., M. Manghi, D. Salerno, A. Tempestini, V. Iadarola, L. Nardo, S. Brioschi, and F. Mantegazza. 2016. Effects of cytosine methylation on DNA morphology: An atomic force microscopy study. Bba-Gen Subjects 1860:1-7.
26. Jimenez-Useche, I., J. Ke, Y. Tian, D. Shim, S. C. Howell, X. Qiu, and C. Yuan. 2013. DNA methylation regulated nucleosome dynamics. Sci Rep 3:2121.
27. Jimenez-Useche, I., and C. Yuan. 2012. The effect of DNA CpG methylation on the dynamic conformation of a nucleosome. Biophysical journal 103:2502-2512.
28. Bustamante, C., Z. Bryant, and S. B. Smith. 2003. Ten years of tension: single-molecule DNA mechanics. Nature 421:423-427.
29. Bustamante, C., S. B. Smith, J. Liphardt, and D. Smith. 2000. Single-molecule studies of DNA mechanics. Curr Opin Struc Biol 10:279-285.
30. Smith, S. B., Y. Cui, and C. Bustamante. 1996. Overstretching B-DNA: the elastic response of individual double-stranded and single-stranded DNA molecules. Science 271:795-799.
31. Bustamante, C., J. F. Marko, E. D. Siggia, and S. Smith. 1994. Entropic elasticity of lambda-phage DNA. Science 265:1599-1600.
32. Bouchiat, C., M. D. Wang, J. Allemand, T. Strick, S. M. Block, and V. Croquette. 1999. Estimating the persistence length of a worm-like chain molecule from force-extension measurements. Biophysical journal 76:409-413.

33. Odijk, T. 1995. Stiff Chains and Filaments under Tension. Macromolecules 28:7016-7018.
34. King, G. A., P. Gross, U. Bockelmann, M. Modesti, G. J. Wuite, and E. J. Peterman. 2013. Revealing the competition between peeled ssDNA, melting bubbles, and S-DNA during DNA overstretching using fluorescence microscopy. Proceedings of the National Academy of Sciences of the United States of America 110:3859-3864.
35. Zhang, X., H. Chen, S. Le, I. Rouzina, P. S. Doyle, and J. Yan. 2013. Revealing the competition between peeled ssDNA, melting bubbles, and S-DNA during DNA overstretching by single-molecule calorimetry. Proceedings of the National Academy of Sciences of the United States of America 110:3865-3870.
36. Takai, D., and P. A. Jones. 2002. Comprehensive analysis of CpG islands in human chromosomes 21 and 22. Proceedings of the National Academy of Sciences of the United States of America 99:3740-3745.
37. Takai, D., and P. A. Jones. 2003. The CpG island searcher: a new WWW resource. In silico biology 3:235-240.
38. Rozen, S., and H. J. Skaletsky. 1998. Primer3. http://www-genome.wi.mit.edu/genome_software/other/primer3.html.
39. Benson, D. A., M. Cavanaugh, K. Clark, I. Karsch-Mizrachi, D. J. Lipman, J. Ostell, and E. W. Sayers. 2013. GenBank. Nucleic acids research 41:D36-42.
40. Bianco, P., Z. Martonfalvi, K. Naftz, D. Koszegi, and M. Kellermayer. 2015. Titin domains progressively unfolded by force are homogenously distributed along the molecule. Biophysical journal 109:340-345.
41. Bianco, P., A. Nagy, A. Kengyel, D. Szatmari, Z. Martonfalvi, T. Huber, and M. S. Kellermayer. 2007. Interaction forces between F-actin and titin PEVK domain measured with optical tweezers. Biophysical journal 93:2102-2109.
42. Kellermayer, M. S., S. B. Smith, H. L. Granzier, and C. Bustamante. 1997. Folding-unfolding transitions in single titin molecules characterized with laser tweezers. Science 276:1112-1116.
43. Martonfalvi, Z., P. Bianco, M. Linari, M. Caremani, A. Nagy, V. Lombardi, and M. Kellermayer. 2014. Low-force transitions in single titin molecules reflect a memory of contractile history. J Cell Sci 127:858-870.
44. Smith, S. B., Y. Cui, and C. Bustamante. 2003. Optical-trap force transducer that operates by direct measurement of light momentum. Methods in enzymology 361:134-162.
45. Schrödinger, L. 2015. Maestro.
46. Jorgensen, W. L., J. Chandrasekhar, J. D. Madura, R. W. Impey, and M. L. Klein. 1983. Comparison of simple potential functions for simulating liquid water. J. Chem. Phys. 79:926–935.
47. Hart, K., N. Foloppe, C. M. Baker, E. J. Denning, L. Nilsson, and A. D. MacKerell. 2012. Optimization of the CHARMM additive force field for DNA: Improved treatment of the BI/BII conformational equilibrium. J. Chem. Theor. Comp. 8:348-362.
48. Phillips, J. C., R. Braun, W. Wang, J. Gumbart, E. Tajkhorshid, E. Villa, C. Chipot, R. D. Skeel, L. Kalé, and K. Schulten. 2005. Scalable molecular dynamics with NAMD. J. Comp. Chem. 26:1781-1802.
49. Satchwell, S. C., H. R. Drew, and A. A. Travers. 1986. Sequence periodicities in chicken nucleosome core DNA. Journal of molecular biology 191:659-675.

50. Fraser, R. M., D. Keszenman-Pereyra, M. W. Simmen, and J. Allan. 2009. High-resolution mapping of sequence-directed nucleosome positioning on genomic DNA. Journal of molecular biology 390:292-305.
51. Bettecken, T., Z. M. Frenkel, and E. N. Trifonov. 2011. Human nucleosomes: special role of CG dinucleotides and Alu-nucleosomes. BMC genomics 12:273.
52. Mirsaidov, U., W. Timp, X. Zou, V. Dimitrov, K. Schulten, A. P. Feinberg, and G. Timp. 2009. Nanoelectromechanics of methylated DNA in a synthetic nanopore. Biophysical journal 96:L32-34.
53. Rivetti, C., and S. Codeluppi. 2001. Accurate length determination of DNA molecules visualized by atomic force microscopy: evidence for a partial B- to A-form transition on mica. Ultramicroscopy 87:55-66.
54. Hormeno, S., B. Ibarra, J. L. Carrascosa, J. M. Valpuesta, F. Moreno-Herrero, and J. R. Arias-Gonzalez. 2011. Mechanical properties of high-G.C content DNA with a-type base-stacking. Biophysical journal 100:1996-2005.
55. Peters, J. P., N. A. Becker, E. M. Rueter, Z. Bajzer, J. D. Kahn, and L. J. Maher, 3rd. 2011. Quantitative methods for measuring DNA flexibility in vitro and in vivo. Methods in enzymology 488:287-335.
56. Japaridze, A., D. Vobornik, E. Lipiec, A. Cerreta, J. Szczerbinski, R. Zenobi, and G. Dietler. 2016. Toward an Effective Control of DNA's Submolecular Conformation on a Surface. Macromolecules 49:643-652.
57. Fu, H., H. Chen, X. Zhang, Y. Qu, J. F. Marko, and J. Yan. 2011. Transition dynamics and selection of the distinct S-DNA and strand unpeeling modes of double helix overstretching. Nucleic acids research 39:3473-3481.
58. Bosaeus, N., A. H. El-Sagheer, T. Brown, B. Akerman, and B. Norden. 2014. Force-induced melting of DNA--evidence for peeling and internal melting from force spectra on short synthetic duplex sequences. Nucleic acids research 42:8083-8091.
59. Zhang, X., Y. Qu, H. Chen, I. Rouzina, S. Zhang, P. S. Doyle, and J. Yan. 2014. Interconversion between three overstretched DNA structures. Journal of the American Chemical Society 136:16073-16080.
60. Nardo, L., M. Lamperti, D. Salerno, V. Cassina, N. Missana, M. Bondani, A. Tempestini, and F. Mantegazza. 2015. Effects of non-CpG site methylation on DNA thermal stability: a fluorescence study. Nucleic acids research.
61. Bosaeus, N., A. H. El-Sagheer, T. Brown, S. B. Smith, B. Akerman, C. Bustamante, and B. Norden. 2012. Tension induces a base-paired overstretched DNA conformation. Proceedings of the National Academy of Sciences of the United States of America 109:15179-15184.

Supporting Information
CpG island hypermethylation increases DNA compliance and stabilizes against mechanical strand separation

Cs. I. Pongor[1], P. Bianco[1,2], Gy. Ferenczy[1,3], R. Kellermayer[4], M. Kellermayer[1,5]

1. Design and characteristics of the DNA construct

The mechanically manipulated DNA construct was prepared by amplifying the 3403 – 6715 fragment of λ-phage DNA (NCBI Reference Sequence NC_001416.1; obtained from New England Biolabs). The total length of the construct was 3312 base pairs. The primers used were 5'-biotin-CGTGCCGGTGTGCAG and 5'-NH_2-CACCGCTGGCGTTCA. The entire sequence, with the primer positions highlighted in bold, the pyrosequenced regions and the inclusive CpG elements (see below) in yellow and red, respectively, and the sequence chosen for molecular dynamics simulation in green, is shown below:

cgtgccg gtgtgcagat taatgacagc ggtgcggcgc tgggatatta cgtcagcgag
gacgggtatc ctggctggat gccgcagaaa tggacatgga taccccgtga gttacccggc
gggcgcgcct cgttcattca cgtttttgaa cccgtggagg acgggcagac tcgcggtgca
aatgtgtttt acagcgtgat ggagcagatg aagatgctcg acacgctgca gaacacgcag
ctgcagagcg ccattgtgaa ggcgatgtat gccgccacca ttgagagtga gctggatacg
cagtcagcga tggattttat tctgggcgcg aacagtcagg agcagcggga aaggctgacc
ggctggattg gtgaaattgc cgcgtattac gccgcagcgc cggtccggct gggaggcgca
aaagtaccgc acctgatgcc gggtgactca ctgaacctgc agacggctca ggatacggat
aacggctact ccgtgtttga gcagtcactg ctgcggtata tcgctgccgg gctgggtgtc
tcgtatgagc agctttcccg gaattacgcc cagatgagct act**ccacggc** **acgggccagt**
gcgaacgagt cgtgggcgta ctttatgggg cggcgaaaat tcgtcgcatc ccgtcaggcg
agccagatgt ttctgtgctg gctggaagag gccatcgttc gccgcgtggt gacgttacct
tcaaaagcgc gcttcagttt tcaggaagcc cgcagtgcct gggggaactg cgactggata
ggctccggtc gtatggccat cgatggtctg aaagaagttc aggaagcggt gatgctgata
gaagccggac tgagtaccta cgagaaagag tgcgcaaaac gcggtgacga ctatcaggaa
atttttgccc agcaggtccg tgaaacgatg gagcgccgtg cagccggtct taaaccgccc
gcctgggcgg ctgcagcatt tgaatccggg ctgcgacaat caacagagga ggagaagagt
gacagcagag ctgcgtaatc tcccgcatat tgccagcatg gcctttaatg agccgctgat
gcttgaaccc gcctatgcgc gggttttctt ttgtgcgctt gcaggccagc ttgggatcag
cagcctgacg gatgcggtgt ccggcgacag cctgactgcc caggaggcac tcgcgacgct
ggcattatcc ggtgatgatg acggaccacg acaggcccgc agttatcagg tcatgaacgg
catcgccgtg ctgccggtgt ccggcacgct ggtcagccgg acgcgggcgc tgcagccgta
ctcggggatg accggttaca acggcattat cgcccgtctg caacaggctg ccagcgatcc
gatggtggac ggcattctgc tcgatatgga cacgcccggc gggatggtgg cgggggcatt
tgactgcgct gacatcatcg cccgtgtgcg tgacataaaa ccggtatggg cgcttgccaa
cgacatgaac tgcagtgcag gtcagttgct tgccagtgcc gcctcccggc gtctggtcac
gcagaccgcc cggacaggct ccatcggcgt catgatggct cacagtaatt acggtgctgc
gctggagaaa cagggtgtgg aaatcacgct gatttacagc ggcagccata aggtggatgg
caacccctac agccatcttc cggatgacgt ccgggagaca ctgcagtccc ggatggacgc
aacccgccag atgtttgcgc agaaggtgtc ggcatatacc ggcctgtccg tgcaggttgt
gctggatacc gaggctgcag tgtacagcgg tcaggaggcc attgatgccg gactggctga
tgaacttgtt aacagcaccg atgcgatcac cgtcatgcgt gatgcactgg atgcacgtaa
atcccgtctc tcaggagggc gaatgaccaa agagactcaa tcaacaactg tttcagccac

tgcttcgcag gctgacgtta ctgacgtggt gccagcgacg gagggcgaga acgccagcgc
ggcgcagccg gacgtgaacg cgcagatcac cgcagcggtt gcggcagaaa acagccgcat
tatggggatc ctcaactgtg aggaggctca cggacgcgaa gaacaggcac gcgtgctggc
agaaaccccc ggtatgaccg tgaaaacggc ccgccgcatt ctggccgcag caccacagag
tgcacaggcg cgcagtgaca ctgcgctgga tcgtctgatg caggggcac cggcaccgct
ggctgcaggt aacccggcat ctgatgccgt taacgatttg ctgaacacac cagtgtaagg
gatgtttatg acgagcaaag aaacctttac ccattaccag ccgcagggca **acagtgaccc**
ggctcatacc gcaaccgcgc ccggcggatt gagtgcgaaa gcgcctgcaa tgacccgct
gatgctggac acctccagcc gtaagctggt tgcgtgggat ggcaccaccg acggtgctgc
cgttggcatt cttgcggttg ctgctgacca gaccagcacc acgctgacgt tctacaagtc
cggcacgttc cgttatgagg atgtgctctg gccggaggct gccagcgacg agacgaaaaa
acggaccgcg tttgccggaa cggcaatcag catcgtttaa ctttaccctt catcactaaa
ggccgcctgt gcggcttttt ttacgggatt tttttatgtc gatgtacaca accgcccaac
tgctggcggc aaatgagcag aaatttaagt ttgatccgct gtttctgcgt ctcttttcc
gtgagagcta tcccttcacc acggagaaag tctatctctc aca**aattccg ggactggtaa**
acatggcgct gtacgtttcg ccgattgttt ccggtgaggt tatccgttcc cgtggcggct
ccacctctga atttacgccg ggatatgtca agccgaagca tgaagtgaat ccgcagatga
ccctgcgtcg cctgccggat gaagatccgc agaatctggc ggacccggct taccgccgcc
gtcgcatcat catgcagaac atgcgtgacg aagagctggc cattgctcag gtcgaagaga
tgcaggcagt ttctgccgtg cttaagggca aatacaccat gaccggtgaa gccttcgatc
cggttgaggt ggatatgggc cgcagtgagg agaataacat cacgcagtcc ggcggcacgg
agtggagcaa gcgtgacaag tccacgtatg acccgaccga cgatatcgaa gcctacgcgc
tgaacgccag cggtg

The total number of guanine (G) or cytosine (C) bases in the construct is 1942, which amounts to a GC content of 59%. The construct sequence was analyzed according to CpG island criteria (1, 2) by using the search engine at http://cpgislands.usc.edu/. The search engine parameters were the following: window size 200 bp; minimal length of CpG island 500 bp; minimal ObsCpG/ExpCpG 0.65; distance between adjacent islands 100bp. The total number of CpG sites is 300. The distribution of the sequence distance, in bp, between consecutive CpG sites is shown in **Fig. S1.**

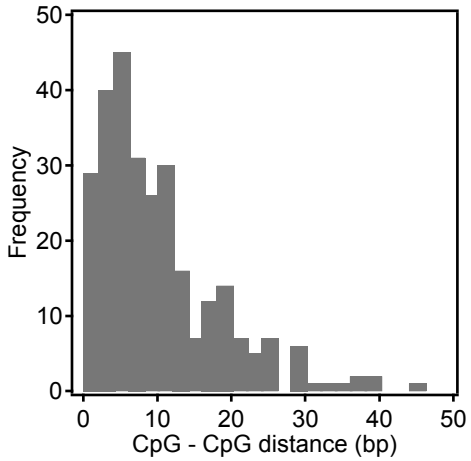

Fig. S1. Histogram of the distance between neighboring CpG sites in base-pair units. Exponential distribution is observed with a mean of 9 bp.

2. Preparation of chemically hypermethylated DNA

Chemically hypermethylated DNA (DNA_{cm}) was prepared by replacing CTP with m^5CTP in the PCR reaction mixture. Because the yield of DNA_{cm} was low in the standard procedure, we added dimethyl sulfoxide (DMSO) to prevent the formation of higher-order template structures and to lower the DNA melting point. The optimum DMSO concentration was between 6-8%, and the resulting yields were almost as high as for non-methylated DNA (DNA_{nm}) (**Fig. S2**).

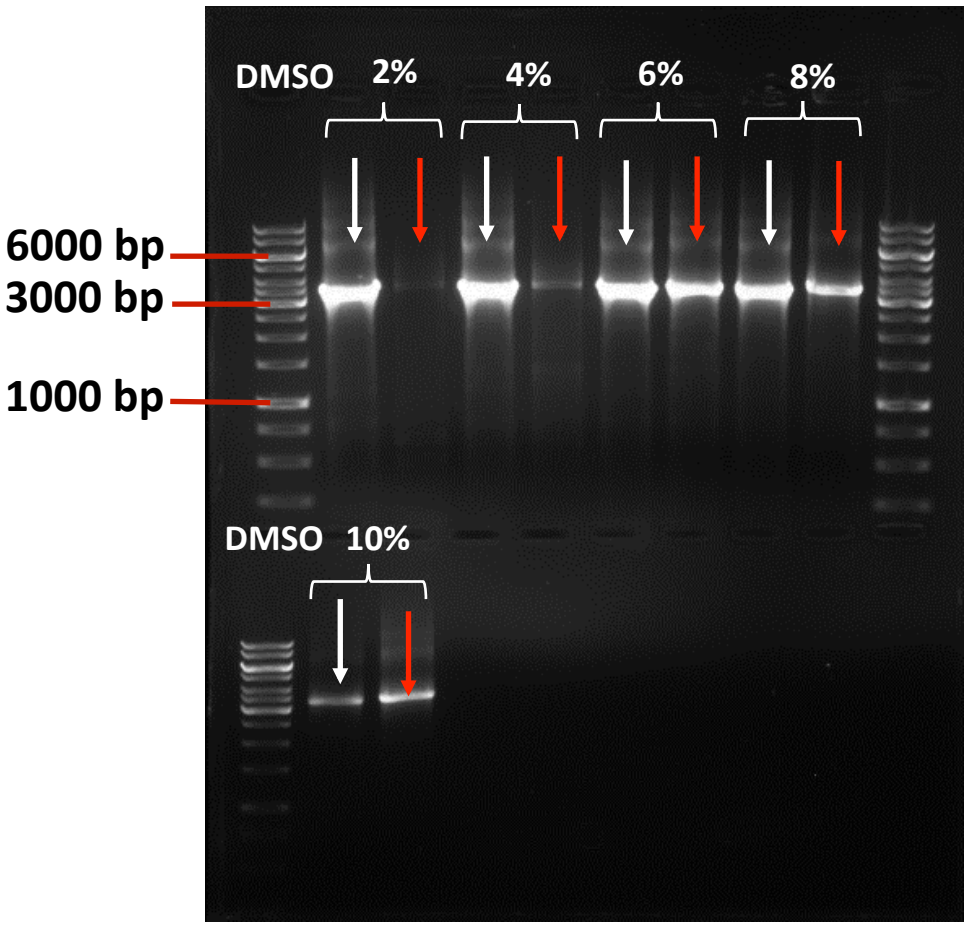

Fig. S2. Gel Photo of PCR products obtained in the presence of different DMSO concentrations. White arrows indicate lanes from PCR reactions containing CTP and red arrows point reaction mixtures containing only m^5CTP instead of CTP.

3. Enyzmatic methylation of DNA

DNA (DNA_{em}) was enzymatically methylated by using M.SssI methyltransferase (Fermentas, Vilnius, Lithuania). The efficiency of the methylation reaction was first analyzed qualitatively with the methylation-sensitive HpaII (Fermentas, Vilnius, Lithuania) nuclease. This nuclease cleaves at CCGG sites, but it does not cleave if the site is methylated. The sequence has 44 cleavage sites in our sequence, which result in fragments of 5-250 bp size. 10 µl of purified DNA was mixed with 2 µl ultrapure water, 2 µl 10x Reaction Buffer and 1 µl HpaII enzyme solution and incubated for 30 minutes at 37°C. The reaction mixtures were analysed using 1% agarose gel electrophoresis in Tris-acetate-EDTA buffer running at 10 V/cm. A gel photo in **Fig. S3** shows the result of the digestion reactions using the non-methylated and enzymatically methylated construct. HpaII completely digested the non-methylated sample while the two methylated samples are almost completely intact proving that most of the cleavage sites where methylated.

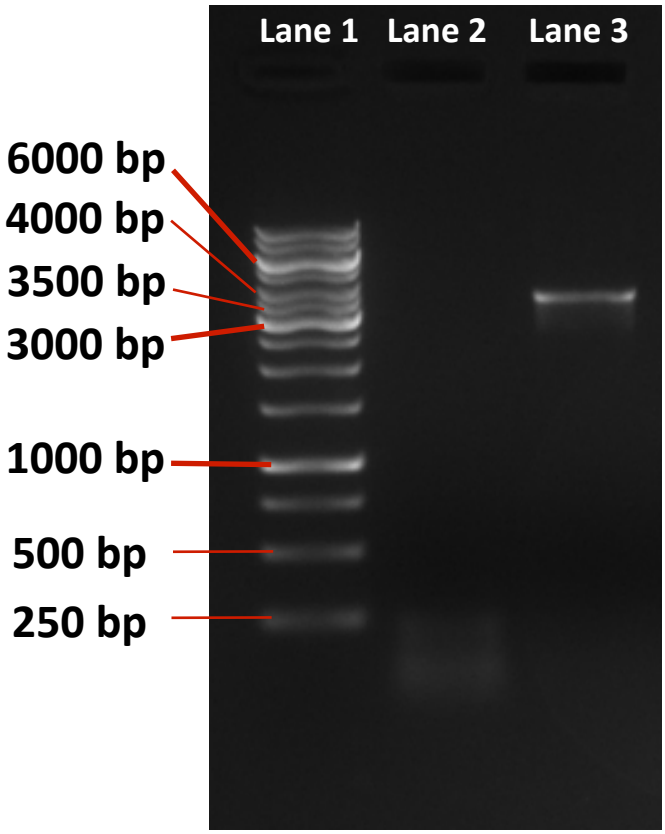

Fig. S3. Gel photo of HpaII digested DNA. Lane 1: 1kb DNA ladder. Lane 2: Non-methylated DNA. Lane 3: Enzymatically methylated DNA.

To obtain a more quantitative assessment of the efficiency of the methylation reaction the enzymatically methylated DNA was also analyzed by pyrosequencing (3) on a PyroMark Q24 sequencer from Qiagen (Venlo, Netherlands). The enzymatically methylated sequence was bisulfite converted by using the EZ DNA Methylation-Direct kit from Zymo Research (Irvine, CA., USA). The sequencing reaction was carried out with a PyroMark Gold Q24 kit from Qiagen (Venlo, Netherlands) using standard protocols. Three regions (see above) where chosen to be analyzed within the sequence that where PCR amplified by using forward and reverse primers. A

60-bp window was sequenced using a sequencing primer in all three cases and bisulfite conversion was checked using control dispersions. The following oligonucleotides were used for the pyrosequencing analysis:

Region 1:

Forward : GGGTTGGGTGTTTAGTATGAGTAGTTTT

Reverse: 5'-biotin-ACTCTACTATCACTCTTCTCCTCCTCTA

Sequencing: GGAATTAAGTTTAGATGAGTTATT

Region 2:

Forward : TGTTGAATATATTAGTGTAAGGGATGTTTATGA

Reverse: 5'-biotin- CCTCCCACCAAAACACATCCTCAT

Sequencing: TTATTATTAGTAGTAGGGTAATAG

Region 3:

Forward : TGTTGGAGGTAAATGAGTAGAAATTTAAGTTTG

Reverse: 5'-biotin- CTACATCTCTTCCACCTAAACAATAACCAACTCTT

Sequencing: GGAGAAAGTTTATTTTTTATA

The distribution of the methylation efficiency is shown below in **Fig. S4.** The methylation efficiency of the 25 CpG cytosines was 89.88±1.29 % (mean ± sem)**.**

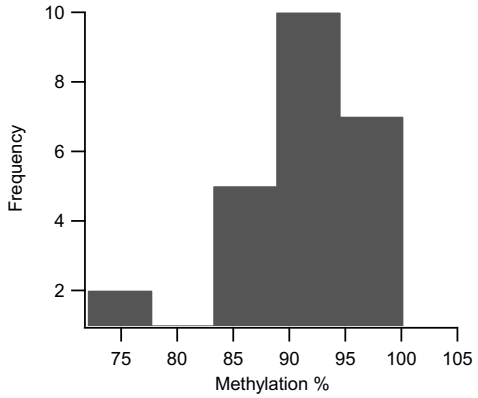

Fig. S4. Histogram showing the efficiency of methylation in the analyzed CpG positions.

4. Contour length analysis of surface-adsorbed DNA molecules

The contour length of the different DNA constructs was also obtained by analyzing AFM images of individual moelcules adsorbed to the surface of freshly cleaved mica (**Fig. S5**). The steps of the analysis are shown in **Fig. S6**. The contour of a DNA molecule was manually drawn by tracing along the axis of the DNA molecule in the AFM image (**Fig. S6b**). The ends of the molecule were defined as the data points at the half-maximal heights in the contour plot (arrows in **Fig.S6c**). Mean contour lengths of the different dsDNA constructs are compared in **Fig. S6d**. The contour length was obtained by measuring the distance between these points along the contour. The distribution of contour length data measured for 32, 38 and 45 molecules of the non-methylated, enzymatically methylated and chemically hypermethylated constructs is shown in **Fig.S6e**.

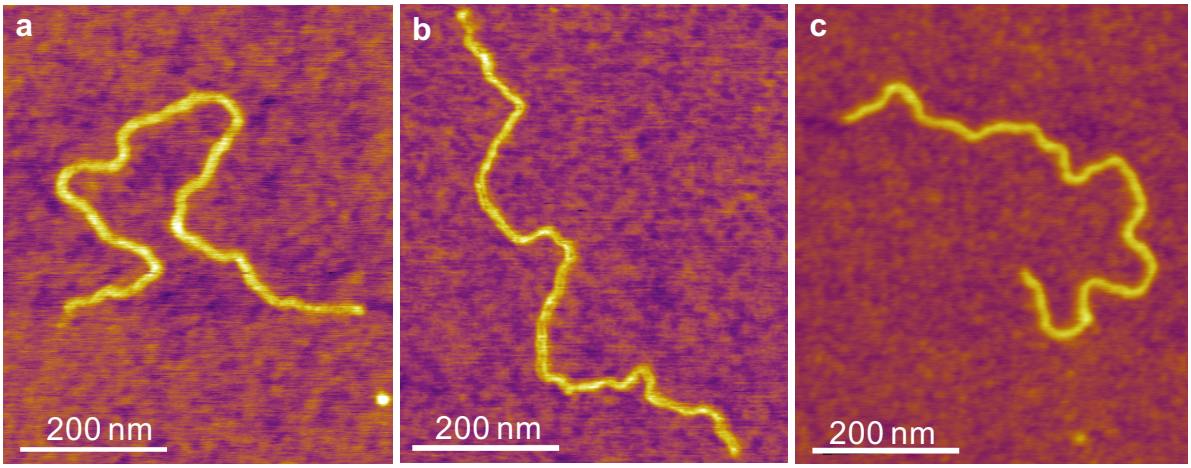

Fig. S5. Atomic force microscopy of surface-adsorbed dsDNA molecules. Representative non-contact-mode AFM images of a $dsDNA_{nm}$ (**a**), $dsDNA_{em}$ (**b**) and $dsDNA_{cm}$ (**c**) molecule.

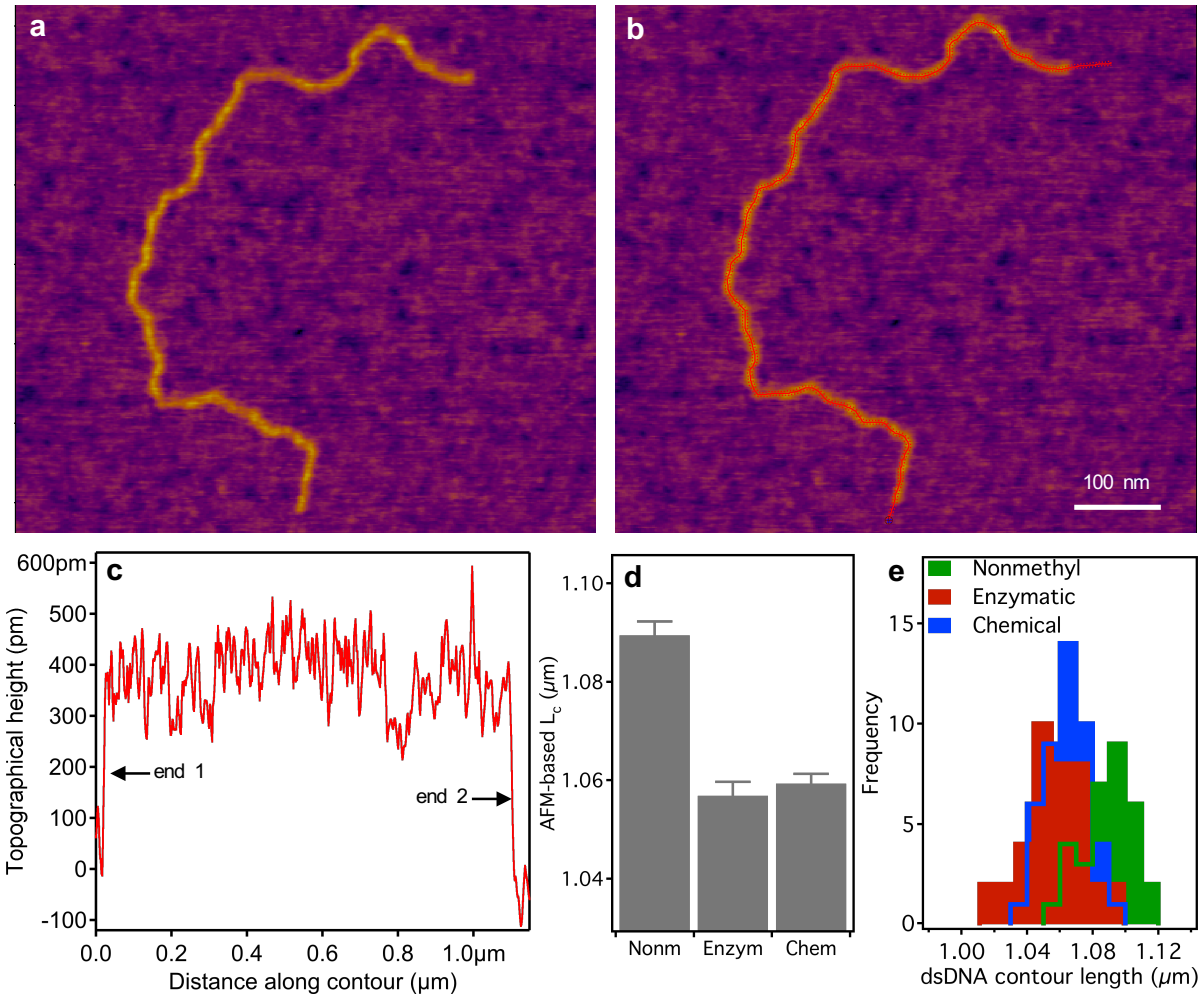

Fig. S6. Analysis of the contour length of individual DNA molecules adsorbed to the surface of mica. **a**. AFM image of a DNA molecule. **b.** AFM image with the contour (red trace), drawn manually, in the axis of the DNA molecule. **c.** Contour plot of the DNA molecule along its axis. **d.** Comparison of the contour lengths, obtained by tracing the AFM images, of the different dsDNA constructs. Error bars refer to S.E.M. Numerical values are presented in **Table 1** of the main text. **e.** Distribution of contour lengths for the non-methylated (green), enzymatically methylated (red) and chemically hypermethylated (blue) constructs.

5. Persistence length analysis of surface-adsorbed DNA molecules

Analysis of the DNA contour on AFM images provides with the possibility to determine the persistence length of the molecules. Considering that both the mean-square separation distance ($<R^2>$) and the mean cosine tangent angle ($<\cos\theta>$) between points along the contour (L) of the chain decay on the scale of the persistence length (L_P) (4), two approaches were employed to estimate the persistence length of the surface-adsorbed dsDNA molecules. After the AFM image was processed to obtain the contour of the molecule (**Fig. S7.a**), in the first approach ("mean-square-separation method") we measured the mean-square linear distance ($<R^2_{s,s+L}>$) between points s and $s+L$ along the contour as a function of contour-length separation (L) (**Fig. S7.b.ii**) according to

$$\left\langle R^2_{s,s+L} \right\rangle = 4L_P\left(L + 2L_P\left(e^{-L/2L_P} - 1\right)\right). \qquad \text{(S1)}$$

In the second approach ("orientation correlation method") we measured the mean cosine angle between tangents ($<\cos\theta_{s,s+L}>$) at contour points located at distances s and $s+L$ as a function of contour-length separation (L) (**Fig. S7.b.iii**) according to

$$\left\langle \cos\theta_{s,s+L} \right\rangle = e^{-L/2L_P}. \qquad \text{(S2)}$$

The persistence lengths calculated for the different dsDNA constructs by using the two different methods are shown in **Fig. S7e**. We note that the persistence lengths calculated for non-methylated dsDNA from the AFM images exceed the one obtained with optical tweezers. Such has been observed before (5), and the high persistence length can be attributed to the high GC content of DNA, which was 59 % in our construct. It is also notable that the AFM-based persistence length of the hypermethylated constructs was greater than that of the non-methylated form. Similar tendencies have been reported recently (6). The persistence-length increase is in contrast with the optical-tweezers measurements where a slight decrement was observed (see **Table 1** of the main text).

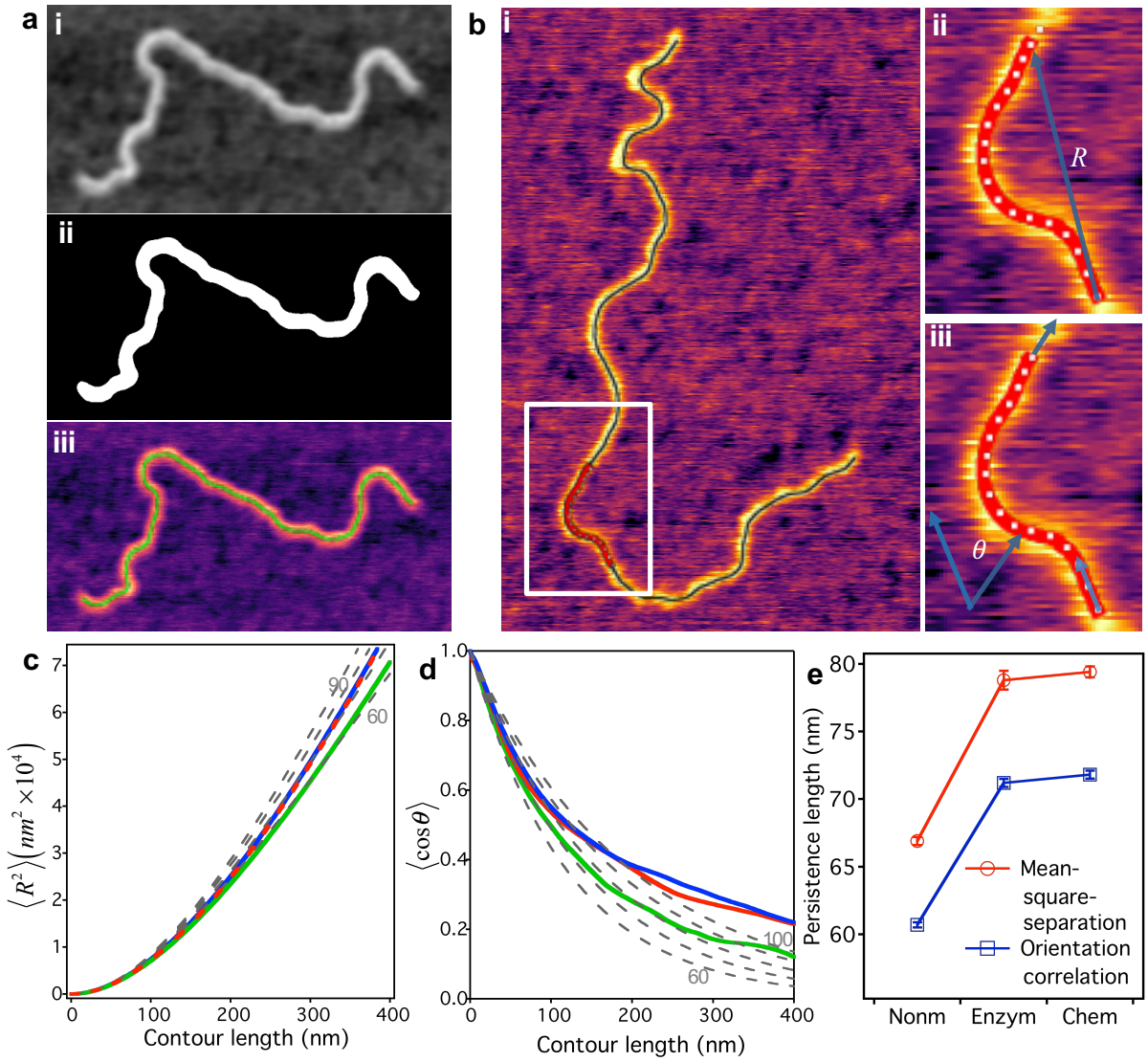

Fig. S7. Persistence length analysis of DNA molecules adsorbed to mica. **a**. Image processing steps for obtaining dsDNA contour: gaussian convolution (**i**), thresholding (**ii**) and skeletonization (**iii**) carried out by using custom Fiji (7) and GNU Octave (8) subroutines. **b.** Shape analysis of dsDNA. The contour was divided into 2.5-nm sections by interpolation (**i**), then the end-to-end distance (R) (**ii**) and tangent angle (θ) (**iii**) were measured between the ends of progressively increasing contour sections. **c.** Mean-square linear distance as a function of contour length for the non-methylated (green), enzymatically methylated (red) and chemically hypermethylated (blue) dsDNA constructs. Segmented lines display, for guiding the eye, theoretical curves for wormlike chains with persistence lengths of 60, 70, 80 and 90 nm. **d.** Mean cosine tangent angle as a function of contour length for the non-methylated (green), enzymatically methylated (red) and chemically hypermethylated (blue) dsDNA constructs. Segmented lines display, for guiding the eye, theoretical curves for wormlike chains with persistence lengths of 60, 70, 80, 90 and 100 nm. **e.** Comparison of the persistence lengths for the different dsDNA constructs by using the different AFM-based methods.

6. Stability and force hysteresis of DNA constructs

The mechanical stability and the magnitude of force hysteresis of the different DNA constructs (DNA_{nm}, DNA_{em}, DNA_{cm}) were investigated in repeated cycles of stretch-relaxation experiment containing phases of force-clamp during which the molecules were held at constant, high forces. The force *versus* extension, force *versus* time and extension *versus* time traces for each of the constructs are shown in **Figs. S8-S10**. **Fig. S11** compares the extension *versus* time functions of the different dsDNA constructs during high-force (80 pN) clamp.

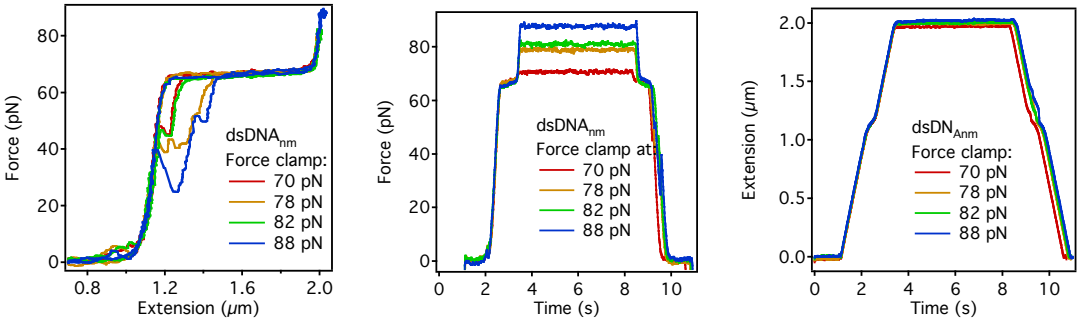

Fig. S8. Nanomechanical traces for DNA_{nm}.

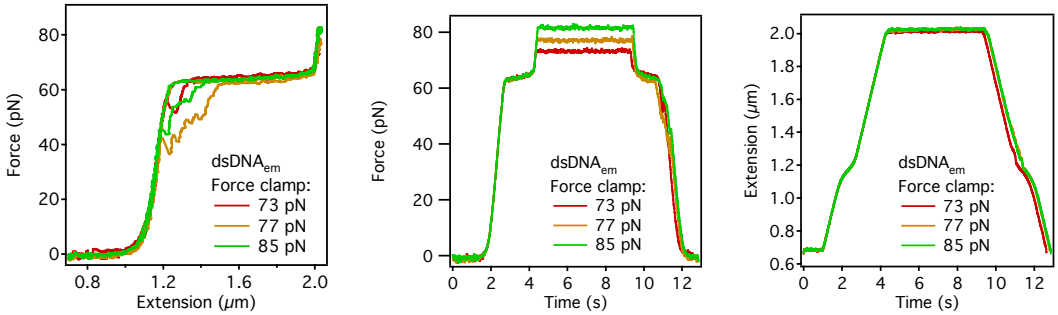

Fig. S9. Nanomechanical traces for DNA_{em}.

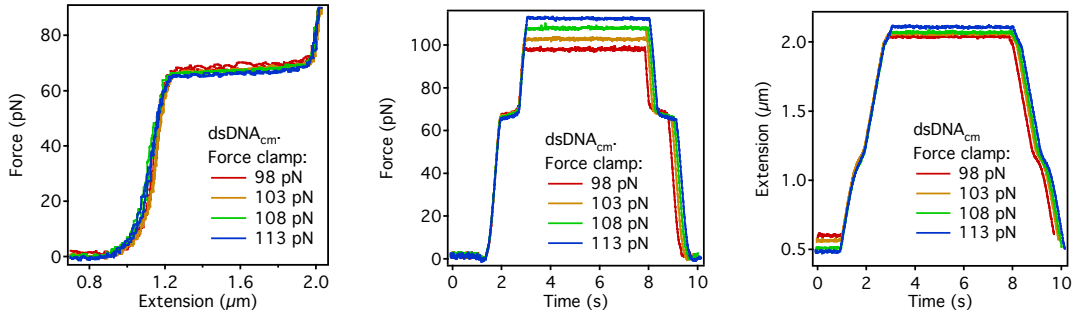

Fig. S10. Nanomechanical traces for DNA_{cm}.

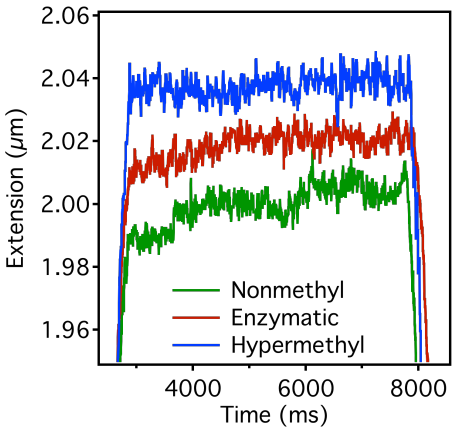

Fig. S11. Extension *versus* time traces for the non-methylated (green), enzymatically methylated (red) and chemically hypermethylated (blue) dsDNA constructs, held at constant, 80 pN force level for 5 s. In these nanomechanical experiments the manipulated DNA molecules have already passed through the overstretch transition.

7. Error analysis of molecular-dynamics simulation data

To assess whether the structural parameters of the modeled non-methylated ($mDNA_{nm}$) and hypermethylated DNA ($mDNA_{cm}$) molecules were significantly different during simulated nanomaniulation, error analyses were carried out. **Fig. S12** below shows the results. The error analysis demonstrates that the difference in extension of $mDNA_{nm}$ and $mDNA_{cm}$ observed in the time period of 2-4 ns, which corresponds to an extension of 50-60 Å beyond the initial end-to-end distance, is significant ($p<0.05$).

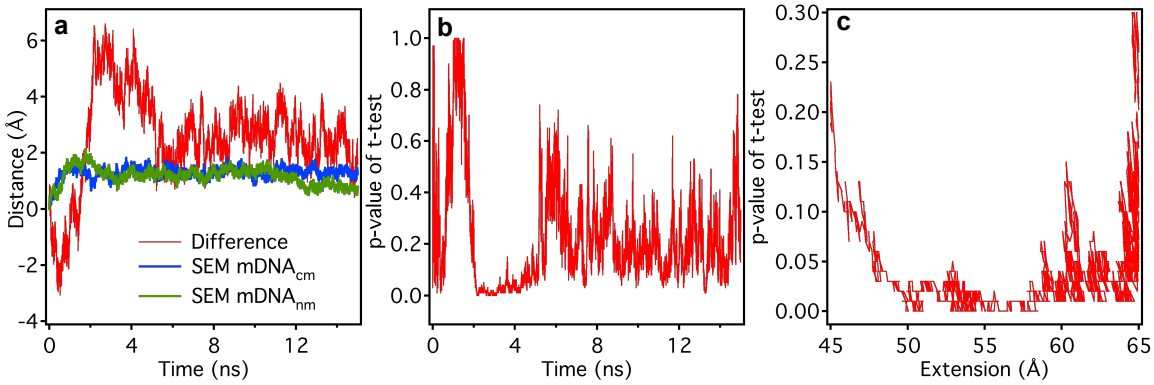

Fig. S12. Error analysis of the force-field molecular dynamics simulation results. **a.** Differences in the mean extension values of $mDNA_{nm}$ and $mDNA_{cm}$ obtained in ten runs of constant force (150 pN) simulation experiments (red) are shown together with the standard error of mean extension for both DNA species. **b.** Time-dependent p values of unpaired t-tests performed for the extensions obtained in the ten simulations for $mDNA_{nm}$ and $mDNA_{cm}$. The p values are below 0.05 in the majority of the 2-4 ns time range. **c.** Extension-dependent p values of unpaired t-tests performed for the extensions obtained in the ten simulations for $mDNA_{nm}$ and $mDNA_{cm}$. The p values are lower than 0.05 in the majority of the 50-60 Å extension range.

8. Distribution of the dsDNA nanomechanical variables

The histograms of the nanomechanical variables shown in **Table 1** of the main text are shown in **Fig. S13**, in order to display the distributions.

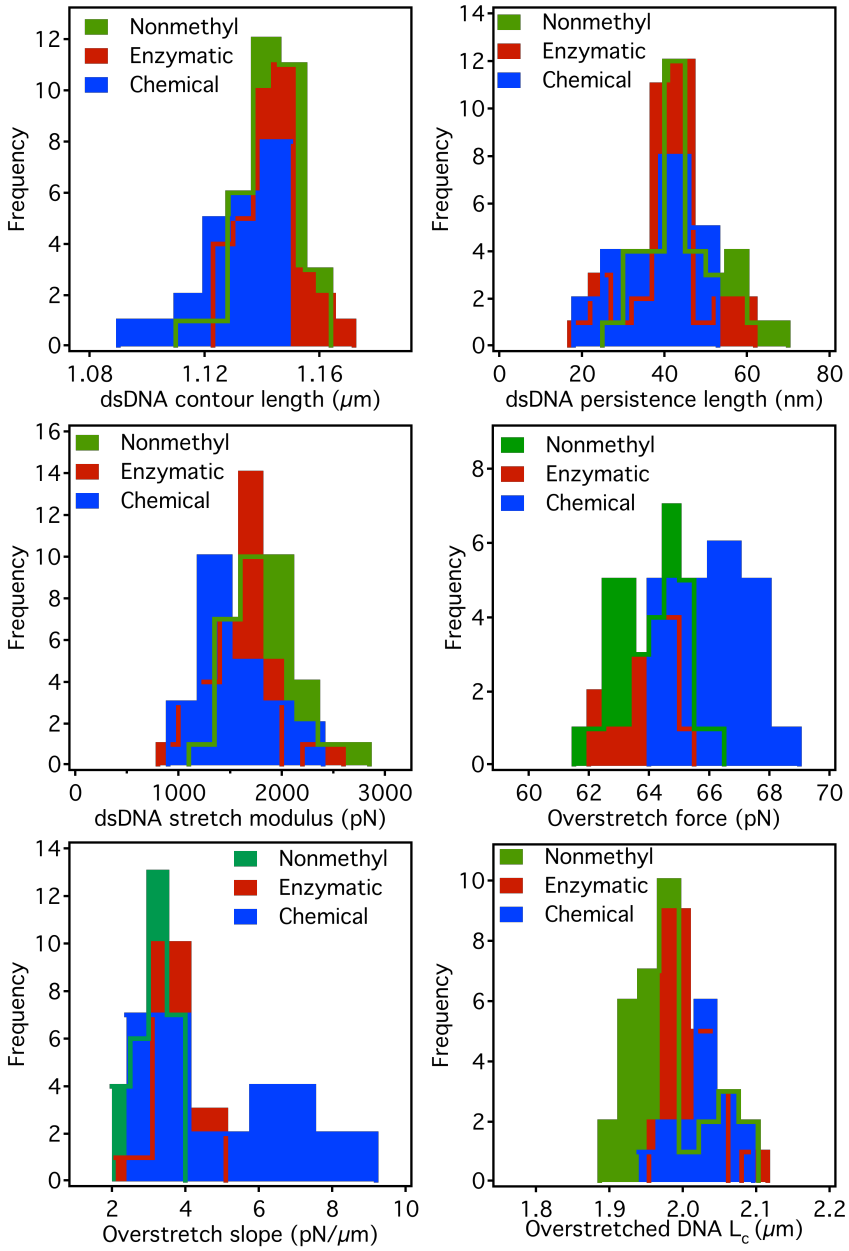

Fig. S13. Distribution of the variables summarized in Table 1 of the main text for the non-methylated, and enzymatically and chemically hypermethylated dsDNA constructs.

The histograms of the magnitude of force hysteresis observed between the stretch and relaxation mechanical half cycles are shown in **Fig. S14.** The hysteresis was quantified either as the distance along the overstretch transition ("hysteresis length") or as the area of the hysteresis expressed in dissipated energy units (pNnm).

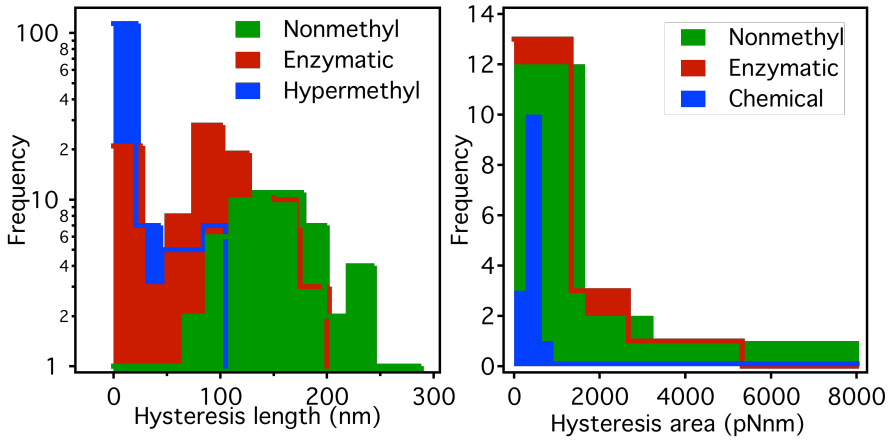

Fig. S14. Distribution of the size of nanomechanical hysteresis for the non-methylated, and enzymatically and chemically hypermethylated dsDNA constructs.

9. Supporting video

Structural changes in 30-bp-long non-methylated ($mDNA_{nm}$) and hypermethylated ($mDNA_{cm}$) DNA molecules. Time-lapse frames corresponding to a 15-ns-long simulation are shown. Red dots indicate intact H-bonds. Passing of time is indicated with the yellow bar.

References

1. Takai, D., and P. A. Jones. 2002. Comprehensive analysis of CpG islands in human chromosomes 21 and 22. Proceedings of the National Academy of Sciences of the United States of America 99:3740-3745.
2. Takai, D., and P. A. Jones. 2003. The CpG island searcher: a new WWW resource. In silico biology 3:235-240.
3. Tost, J., and I. G. Gut. 2007. DNA methylation analysis by pyrosequencing. Nat Protoc 2:2265-2275.
4. Rivetti, C., M. Guthold, and C. Bustamante. 1996. Scanning force microscopy of DNA deposited onto mica: equilibration versus kinetic trapping studied by statistical polymer chain analysis. Journal of molecular biology 264:919-932.
5. Hormeno, S., B. Ibarra, J. L. Carrascosa, J. M. Valpuesta, F. Moreno-Herrero, and J. R. Arias-Gonzalez. 2011. Mechanical properties of high-G.C content DNA with a-type base-stacking. Biophysical journal 100:1996-2005.
6. Cassina, V., M. Manghi, D. Salerno, A. Tempestini, V. Iadarola, L. Nardo, S. Brioschi, and F. Mantegazza. 2016. Effects of cytosine methylation on DNA morphology: An atomic force microscopy study. Bba-Gen Subjects 1860:1-7.
7. Schindelin, J., I. Arganda-Carreras, E. Frise, V. Kaynig, M. Longair, T. Pietzsch, S. Preibisch, C. Rueden, S. Saalfeld, B. Schmid, J. Y. Tinevez, D. J. White, V. Hartenstein, K. Eliceiri, P. Tomancak, and A. Cardona. 2012. Fiji: an open-source platform for biological-image analysis. Nat Methods 9:676-682.
8. Eaton, J. W., D. Bateman, H. Soren, and R. Wehbring. 2015. GNU Octave (version 4.0.0) manual: a high-level interactive language for numerical computations.